Manuscript submitted to *Building and Environment* 2022

Reconfigurable Origami-Inspired Window for Tunable Noise Reduction and Air Ventilation

Xiaomeng Jin[1,2], Hongbin Fang[1,2,3,*], Xiang Yu[4], Jian Xu[1,2], and Li Cheng[4]

1. Institute of AI and Robotics, Fudan University, Shanghai 200433, China
2. MOE Engineering Research Center of AI & Robotics, Fudan University, Shanghai 200433, China
3. Shanghai Key Laboratory of Medical Imaging Computing and Computer Assisted Intervention, Fudan University, Shanghai 200433, China
4. Department of Mechanical Engineering, The Hong Kong Polytechnic University, Hung Hom, Kowloon, Hong Kong, China

[*]**Author for correspondence:** fanghongbin@fudan.edu.cn (H. Fang)

Address: Room 603 Xijinjinbo Building, 539 Handan Rd., Yangpu District, Shanghai 200433, China.

Abstract

Conventional windows encounter significant challenges in simultaneously achieving noise reduction and ventilation. Recent advent in origami technology offers new possibilities and smart solutions to solve this bottlenecking problem. In this paper, we propose a novel modular-origami-based reconfigurable silencing window that achieves balanced noise mitigation and air ventilation while ensuring flexible tunability. Specifically, the balance between the two competing functions originates from the unique 'tile—void' structure of the modular origami, and the tunability is a result of the single-degree-of-freedom folding mechanism. Based on a comprehensive understanding of the correlations between the design variables (including origami geometry, internal partition forms, and folding angles) and the acoustic characteristics of the window, on-demand sound attenuation for a specific target frequency band can be achieved via optimization. Broadband noise reduction can be obtained through cascading multiple origami layers, whose design can be conceived by an intuitive spectral superposition principle. Finally, we demonstrate through numerical simulations that for different working scenarios, balanced sound attenuation and air ventilation can be achieved by simply folding the origami window. This conceptual design, alongside the reported findings, provides new ideas for the design of modular acoustic devices and contributes to addressing the noise reduction and ventilation needs for urban buildings as well as industrial installations.

Keywords: Modular origami, origami acoustics, transmission loss, mean age of air, tunability

1. Introduction

With accelerated urbanization and increased urban population, the adverse effects of traffic noise, construction noise, and community noise generated by human activities become increasingly problematic. A series of studies have shown that prolonged exposure to high levels of noise not only leads to sleep disorders [1], learning disabilities [2–4], causes negative emotions [5,6], and reduces work performance [7–10], but also triggers diseases such as hypertension and cardiopathy [11–13], which impair human health. The control of urban noise is a challenging topic which requires comprehensive efforts. Several studies have pointed out that traffic noise (e.g. road traffic, [14–16] railway traffic [17], air traffic [18,19] and port activities [20–23]) have become a major source of noise that affect human life quality. The most effective way to reduce noise is through source mitigation. Some vehicles incorporate low-noise emission design [24–30]; some roads adopt, for example, asphalt surfaces to reduce noise from vehicle movements [31]; and rail-damping technologies are used to reduce vibration noise when trains pass by [32]. However, it is difficult to completely eliminate traffic noise at the source. Installing noise barriers to block the sound transmission is a common engineering practice, but generally only on major expressways and high-speed railroads due to the high cost incurred. Windows that can muffle sound is the last line of defense against noise.

People spend most of their time indoors [33,34]. A quiet indoor environment produces better acoustic comfort, improves sleeping quality, and promotes physiological and psychological well-being [6,35]. Noise mainly transmits into the room through windows. Although closed window can block noise transmission effectively, an open window allowing for natural ventilation is preferred by many people as long as the associated noise ingress is reasonably controlled. This, however, poses great challenges as natural ventilation and noise insulation compete with each other which can hardly be conciliated without due and meticulous consideration. In addition, environmental noise is usually broadband in nature [36,37], containing variable frequency contents [38–40] and tidal characteristics [41]. This imposes additional requirements on the performance and calls for the tunability of the window. Meanwhile, the main function of a window may also vary at different times of the day. For example, the traffic noise is significant during the daytime, and the primary duty of the window is

noise reduction; while at night, the traffic noise is substantially reduced, and enhancing air circulation might become an important requirement to maintain a comfortable sleep [35].

Air ventilation and noise reduction are two functions that are competing with each other in conventional windows. Opening the window allows for natural ventilation, but the noise will enter the room without hindrance. Incorporating mechanical ventilation to design noise-insulation windows may ease the problem. By using fans or other mechanical means to circulate air [42,43], mechanical ventilation requires a smaller opening area with higher air exchange rate, but it often introduces new noise sources and consumes more energy. Staggered structures or plenum windows [44–49] provide an alternative way to design naturally-ventilated soundproof windows. A staggered structure is composed of double or multiple glazing separated by a certain distance; the inner and outer layers of the glass have inward and outward openings, respectively, with their positions being staggered. Such a design forces sound waves to go through a Z-shaped channel before entering the room. In the low-to-mid frequency range, noise transmission is reduced by the cavity resonance effect; while at higher frequencies, the silencing effect is determined by the geometry relationship and the damping materials applied along the sound channel [50]. To improve noise insulation, sound-absorbing materials such as foam and micro-perforated panels [45,50–55] have been included in the channel between the double glazing, and acoustic barriers [45,50] can be added to shield the inner and outer openings of the window. In addition, active noise cancellation (ANC) technology [56,57] has been applied to staggered windows to specifically tackle low-frequency noise and extend the working frequency range of the staggered windows [58–62]. Although ANC can achieve more than10 dB noise reduction in the targeted frequency, the increasing complexity and the bulkiness of the system hinder its applicability in window structures. Meanwhile, the durability and reliability of the ANC system is also seen as a major problem under more severe working conditions [63].

As a passive means, introducing acoustic resonators into windows has been attracting persistent attention. By embedding soundproof ventilation units, usually composed of rectangular or parallelepiped cavities, doors and windows that are capable of ventilating air and reducing noise have been designed [64,65]. Airflow-transparent soundproof windows comprising a three-dimensional array of resonators have been proposed [66,67], which combine the acoustic diffraction theory and the acoustic metamaterial theory. More than 20 dB noise reduction can be achieved in the frequency range

of 400-5000 Hz with 20 mm circular air openings [66], which can be narrowed down to 700-2200 Hz with 50 mm air openings [66], and 600-1600 Hz with 60 mm square openings [67]. The application of acoustic metamaterials and acoustic metasurfaces has also led to more diverse designs of silencing windows. Moreover, several studies have demonstrated that porous materials and acoustic metamaterials can entail silencing and ventilation simultaneously [68–75]. However, the resonator designed to suppress noise requires small ventilation channels, thus limiting the opening ratio and compromising air exchange rate. A series of soundproof windows that can effectively reduce noise in a wide frequency range [33,76–79] have been devised, whilst providing a sufficient opening ratio. Some windows have also been improved to allow for visual connections to the outside world [78,79]. However, the existing passive designs and solutions also lack the flexibility to handle noise with variable frequency or adjust the ventilation performance on demand. This, therefore, calls for novel window design solutions to achieve effective ventilation, broadband and adjustable noise reduction.

The development of origami science has provided a wealth of inspiration to engineering designs, and the tunability originating from folding has received extensive attention in many scientific fields including acoustics. For example, Thota et al. [80–82] used the Miura-origami sheet as a platform to adjust the topological properties of a lattice formed by circular tubes attached to the origami sheet, which is exploited to develop tunable sound barriers that can attenuate traffic noise with a complex frequency spectrum. Cambonie and Gourdon [83] proposed an innovative origami solution for an enhanced quarter-wavelength resonator. By adjusting the folding angle of the origami spiral inserted into a resonator, the absorption characteristics of a longer-wavelength resonator can be obtained in a shorter dimension. Zhu et al. [84] designed an origami-based reconfigurable acoustic metamaterial for controllable sound wave manipulation. By adjusting the shape of the constituent origami units, various acoustic manipulation functionalities, including acoustic focusing, beam splitting, sound localization, and unidirectional transmission, can also be achieved. In our previous research [85], a novel modular-origami-inspired muffler with unique acoustic adjustability and programmability has been designed and prototyped. Through a single-degree-of-freedom folding reconfiguration, the working bandwidth of the muffler can be effectively tailored; further, by combining multiple origami layers and through optimization, multi-layer origami mufflers can also be designed to cope with a specific target frequency band. Based on this concept, Fusaro et al. [77] have designed a broadband reconfigurable silencing

window, which integrates the basic resonating principle, auxetic mechanism, and layering technique to achieve noise and air control. In addition to the above work, origami has also inspired the development of other reconfigurable devices for achieving enhanced acoustic tunability and programmability, such as tunable Helmholtz resonators [86], adaptive acoustic tanks for reflection mitigation [87], origami sound absorbers [88], foldable sound barriers [89], reconfigurable acoustic waveguides [90,91] and origami partitions for open-plan spaces [92], etc.

The above success motivates us to extend the previously proposed concept of a single-channel origami muffler to an origami silencing window and, by capitalizing on the advantage of the structural features and foldability of the origami, to achieve a tunable and balanced functionality in terms of ventilation and noise reduction. Specifically, based on a modular origami, we expect to realize effective noise reduction by constructing, optimizing, and cascading resonance cavities, and to achieve excellent tunability of ventilation and noise attenuation performance through changing the shape and the size of the ducts in a foldable manner. To meet this goal, the following studies are conducted. First, by extending the modular-origami structure in the plane and by introducing different partitions into the chambers, origami windows with three partition forms are designed (Section 2). The size and the shape of the ventilation ducts can be effectively tuned via a single-degree-of-freedom folding mechanism. Second, through a comprehensive parameter study of the origami geometries, partition forms, and folding angles, the acoustic characteristics of the silencing window are revealed, based on which, discrete numerical optimizations are carried out to determine the optimal layout entailing maximum average transmission loss for a given target frequency band (Section 3). The results indicate that the single-layer origami window performs poorly in achieving broadband sound suppression. To overcome this limitation, the feasibility and effectiveness of cascading multiple geometrically compatible modular-origami layers are examined in Section 4. Based on an intuitive spectral superposition principle, the layout of the constituent layers can be determined, and the constructed dual-layer window achieves broader bandwidth in noise reduction. Finally, the ventilation characteristics of the window are evaluated (Section 5). It shows that folding endows the origami window with extraordinary tunability in response to different working conditions, therefore achieving the balance between noise reduction and air ventilation that has long been desired.

2. Design of the origami silencing window

Inspiration for this study comes from *modular origami*, which first fold multiple paper stripes into modules and then connect them into a 3D interlocked assembly [93,94]. Transformable modular origami structures are of particular interest to researchers due to their high reconfigurability and extensibility [94,95]. Figure 1(a) shows the photo of a typical modular origami structure, a cube assembly, which can be transformed among different configurations. Treating the cube assembly as a 2D shape, it can then be described as a 2D tiling pattern consisting of four interconnected 'tiles' surrounding a 'void' (Fig. 1(b)). By folding the modular origami via a single-DOF mechanism (i.e., changing the folding angle θ), the shape of the 'void' can transform from a square to a rhombus, and finally to a closed state (Fig. 1(a)). Correspondingly, the area of the void (S_{Void}) decreases significantly, which is the basis for subsequent realization of ventilation regulation; and the area ratio between the 'tiles' and the 'void' ($\gamma = S_{\text{Tiles}} / S_{\text{Void}}$) increases, which makes it possible to tune the sound attenuation. Note that a single modular-origami unit can be periodically tessellated into a 2D origami surface (Fig. 1(d)), which forms the basis of the origami window design.

Fundamentally, an analogy between the modular origami and a silencer design can be drawn, i.e., the 'void' corresponds to the acoustic duct, and the square 'tiles' correspond to the acoustic chambers (Fig. 1(b)) [85]. If we directly tesselate the single modular-origami unit to form a silencing window, some ducts are not connected with any chambers, thus causing sound leakage (Fig. 1(d)). To tackle this problem, the connectivity between the ducts and the chambers of the origami window is redesigned by connecting each duct to only one chamber. Figure 1(e) depicts the 2D design sketch and 3D model of the silencing window. As illustrated by two basic units, each unit consists of a rhombus duct and a square chamber. The 2D geometry of the origami window can be described by the side length a and the folding angle θ of the basic unit, alongside the number of units in each row and column. Note that although the window shown in Fig. 1(e) possesses 7×7 units, it can still be reconfigured, transiting between the fully-open state ($\theta = 90^\circ$) to the fully closed state ($\theta = 0^\circ$) with a single DOF.

On the basis of the basic unit composed of chamber and duct, partitions can be further added into the chambers to increase the design freedom and enhance the low-frequency silencing effect [96]. Figure 2 illustrates three partition forms, which are referred to as PF1, PF2, and PF3, respectively; the

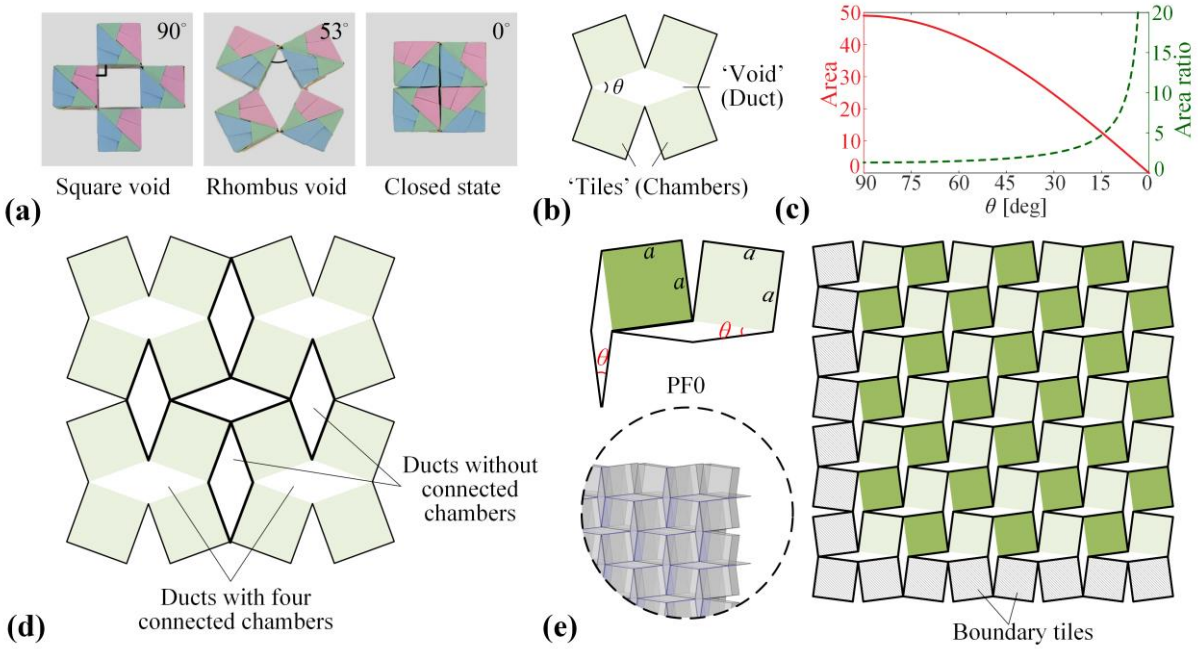

Figure 1. Design of the modular-origami window. (a) Folding of a paper modular origami prototype, from the state with a square void to a state with a rhombus void, and to the closed state. (b) Correspondence between the modular origami and the origami silencer. (c) Variation of the void area and the area ratio with folding. (d) Direct expansion of the modular origami into a plane, in which some ducts are not connected with any chambers. (e) 2D and 3D design of the origami window (PF0), in which the two basic units are demonstrated in the enlarged view. Note that additional closed chambers (denoted by shades of gray) are added at the left and bottom boundaries to ensure periodicity.

case without internal partition is referred to as PF0. Specifically, in a 2D view, PF1(Fig. 2(a)) is a line segment drawn from the center of the square chamber to the obtuse vertex of the rhombus duct, and its length is half of the diagonal of the square (i.e., $\sqrt{2}a/2$); PF2 (Fig. 2(b)) is an 'L'-sharped polyline that follows the shared edge of the square and then bend to the square center, and the lengths of both segments are $a/2$. PF3 (Fig. (2c)) is a spiral-like polyline that starts from the acute vertex of the rhombus duct, then turn into the interior of the chamber, and again turns twice around the square center; the lengths of the four segments are $2a/3$, $2a/3$, $a/3$, and $a/3$, respectively. In a similar way to Fig. 1(e), three types of 7×7 origami window can be constructed by periodically tessellating the units with partition forms PF1, PF2, and PF3, shown in Fig. 2(e)-(f). Note that the insertion of the partition can effectively change the equivalent length of the waveguide and thus adjust the sound-suppression frequency characteristics of the origami window.

In addition to the 2D dimension, the thickness of the chamber w and the lengths of the duct beyond the anechoic layer are defined. If the origami window contains a single anechoic layer, the

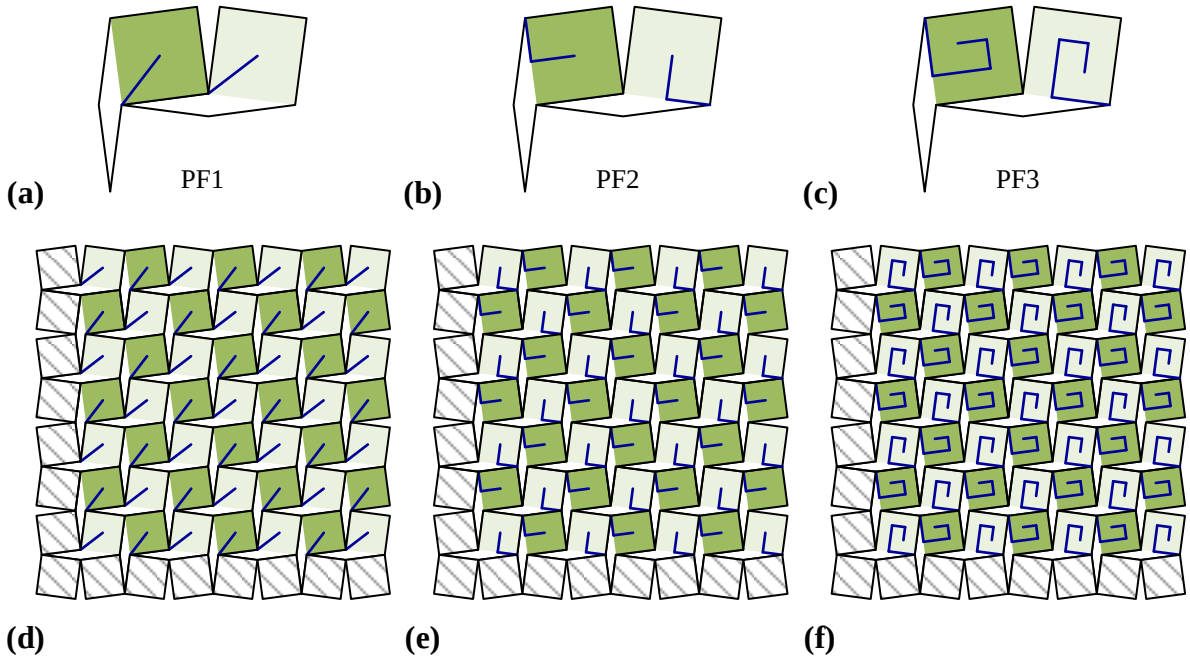

Figure 2 Partition configurations and the corresponding origami silencing window designs. (a) and (d) PF1, in which a line partition is included; (b) and (e) PF2, in which an 'L'-shaped partition is included; (c) and (f) PF3, in which a spiral-like partition is included. The dark and light green squares denote the two basic units. Additional closed chambers are added at the left and bottom boundaries (hatched squares) to ensure periodicity.

length of the front duct is denoted by l_1 (taking the incident sound field as the front), and the length of the back duct is denoted by l_2 (Fig. 3(a)). Furthermore, if the constituent modular origami cells of the anechoic layers share the same external dimension (i.e., a and θ), it is possible to construct a multi-layer origami silencing window by combining multiple layers with identical/different partition forms together. Taking a double-layer silencing window (Fig. 3(b)) as an example, the two layers share the same side length a, the thickness of the two layers is denoted by w_i $(i=1,2)$, the length of the front duct is l_1, the length of the middle duct between the two layers is l_2, and the length of the back duct is l_3.

It is well known that the ducts beyond the anechoic layer could significantly affect the noise reduction effect. Considering that the focus of this research is the effects of the origami layer, including the size and the partition forms, on the noise reduction, the duct lengths are taken as constants. For the single-layer window, $l_1=5\text{mm}$ and $l_2=125\text{mm}$; for the double-layer model, $l_1=l_3=5$ mm, and $l_2=110$ mm.

3 Modeling and optimization of the origami silencing window

Based on the previously discussed design, this section studies the effects of the geometric parameters and the partition configurations on the resultant silencing performance. Both single-layer and double-layer origami windows are considered.

3.1 Simulation setting

Due to the complex geometry of the origami window, Finite Element Method (FEM) models (Fig. 3) are built using the commercial simulation software COMSOL Multiphysics 5.4. A hemispherical background pressure field is used as the incident domain and plane wave with unity pressure amplitude propagating towards the silencing window is defined to simulate the external noise. The left plane of the window is treated as the incident surface, and sound waves transmit through the origami window before radiating into the semi-infinite space on the right. The acoustic domain is discretized into free-tetrahedral elements, with a maximum mesh size of 0.045m defined according to the minimum acoustic wavelength of interest. With harmonic excitation, the governing Helmholtz equation in terms of the acoustic pressure p writes:

$$\nabla^2 p + k^2 p = 0, \tag{1}$$

where k is the wave number. All the walls and partitions in the model are assumed to be acoustically rigid such that the acoustic waves are completely reflected at the boundaries without any energy loss.

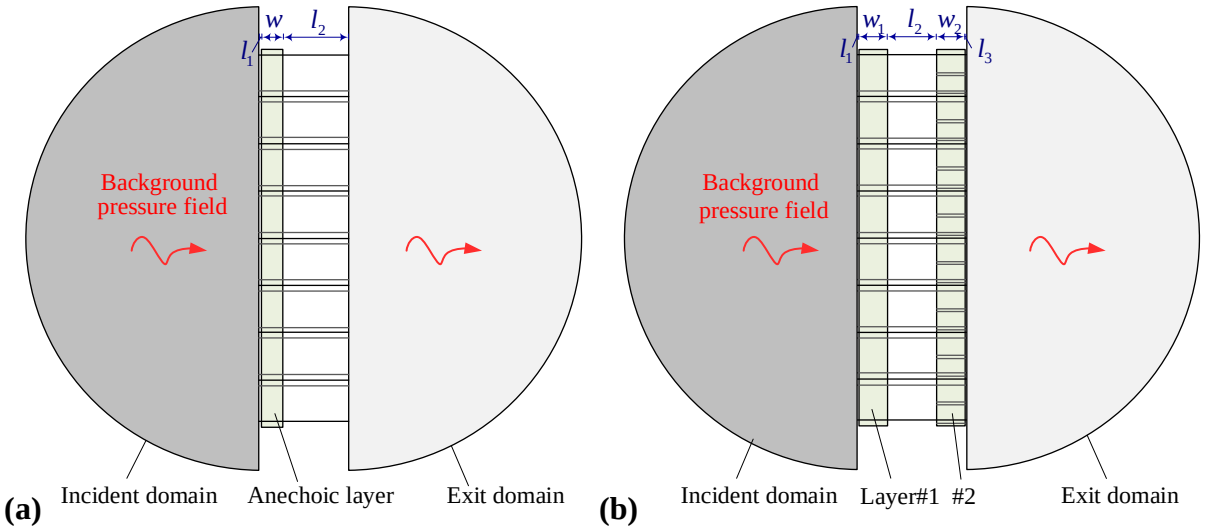

Figure 3. Simulation setup of the origami silencing windows. (a) The window with a single origami anechoic layer; (b) the window with two origami anechoic layers.

The transmission loss (TL) is used to evaluate the difference between the power of the incident wave (W_{in}) at the incident surface and that of the emitted wave at the exit hemispherical surface (W_{out})

$$\mathrm{TL} = 10\log_{10}(W_{in}/W_{out}). \quad (2)$$

A threshold level of 10dB ($\mathrm{TL} \geq 10\mathrm{dB}$), corresponding to an attenuation of the sound power by 90%, is used to define the effective noise reduction band.

3.2 Noise reduction performance of the single-layer silencing window

To understand the effects of the design parameters and the shape of the partitions, a comprehensive parametric analysis is carried out, in which the geometric parameters (the side length a, the chamber thickness w, and the folding angle θ) and the four partition forms (PF0, PF1, PF2, and PF3) of the single-layer silencing window are focused. Figure 4 displays the TL curves corresponding to different window configurations. Specifically, each row corresponds to the same partition form; the first column shares the same chamber thickness ($w = 40\mathrm{mm}$) and folding angle ($\theta = 15^\circ$), with the chamber side length a varying from 70, 75, 80, 85 to 90 mm; the second column has the same side length ($a = 80$ mm) and folding angle ($\theta = 15^\circ$), but with different thicknesses (w varies among 20, 30, 40, 50 and 60 mm); the third column has the same geometries ($w = 40\mathrm{mm}$, $a = 80$ mm) but with different folding angles (θ changing from 15°, 30°, 45°, 60° to 90°).

Overall, Fig. 4 shows that for all partition forms, the incorporated single layer of chambers generate distinct TL peaks to reduce the transmitted noise within a certain frequency band, and the four variables (i.e., the partition form, the chamber thickness w, the chamber side length a, and the folding angle θ) impose great influences on TL. For a given partition form (i.e., in the same row of Fig. 4), the peak frequency of the TL curve shifts towards lower frequency with greater chamber side length a, but it is less sensitive to the chamber thickness w and the folding angle θ. This phenomenon is understandable because the TL peak is caused by the Helmholtz resonance, whose resonance frequency is closely related to the characteristic length of the resonator. At the TL peak, impedance mismatch associated with the Helmholtz resonance prevents sound transmission to the downstream. For example, with PF0, by increasing a from $70\mathrm{mm}$ to $90\mathrm{mm}$, the peak frequency of the TL curve decreases from 1070Hz to 830Hz; however, by changing w and θ, the peak frequency is slightly affected. On the other hand, the breadth of the TL=10 dB band is closely related

to the thickness w and the folding angle θ. With PF0, the effective bandwidth experiences a significant increase from 190 Hz when $w = 20$ mm to 870 Hz when $w = 60$ mm; by folding the window from 90° to 15°, the bandwidth also expands by 8.29 times from 70 Hz to 580 Hz.

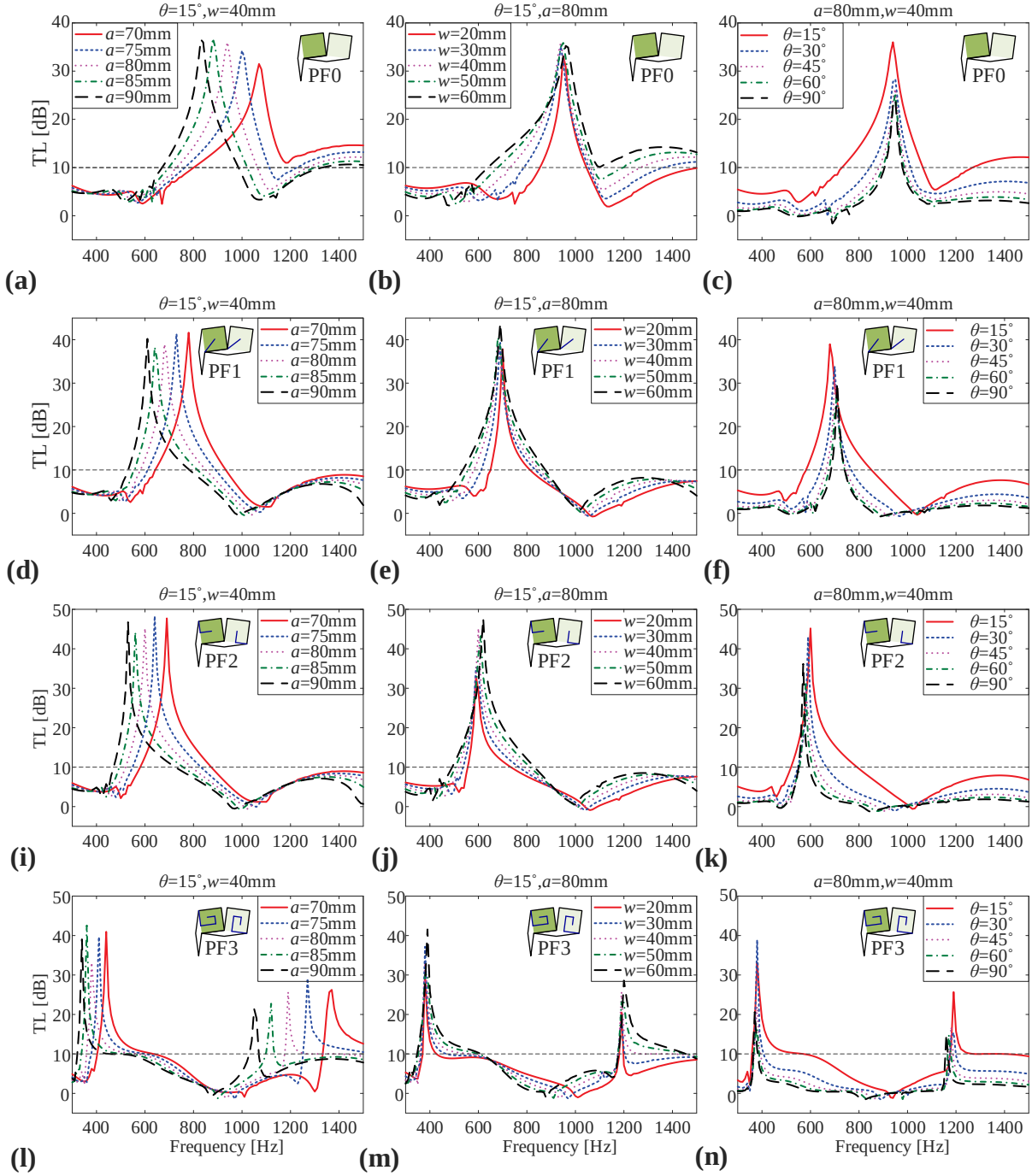

Figure 4. TL curves of the single-layer origami silencing window with different parameters and partition forms. (a)~(c) PF0, (d)~(f) PF1, (i)~(k) PF2, (l)~(n) PF 3. (a), (d), (i), and (l) $\theta = 15^\circ$, $w = 40$ mm; (b), (e), (j), and (m) $\theta = 15^\circ$, $a = 80$ mm; (c), (f), (k), and (n) $a = 80$ mm, $w = 40$ mm. The TL=10dB lines are indicated to show the effective bandwidth.

Cross-comparison among the four rows reveals that the internal partition has significant effects on both the peak frequency and the effective bandwidth of the TL curves. With internal partitions, the equivalent length of the chamber is increased, which, as a result, shifts the TL peaks toward low frequency. However, this is accompanied by the narrowing of the effective bandwidth. For example, the peak frequency of the PF0 window corresponding to $a = 80$ mm, $w = 40$ mm, $\theta = 15^\circ$ is 940 Hz (Fig. 4(a)), while that of the PF 2 window of the same geometries is 600 Hz (Fig. 4(i)). It should be noted that with PF3 (Fig. 4 (k), (l), and (i)), the TL curve possesses two peaks, due to the excitation of higher-order modes.

Figure 4 not only elucidates the effects of the design parameters on the TL performance but also indicates the tuning potentials of the origami window by geometry tailoring. For example, both the peak frequency and the bandwidth can be tuned by adjusting the side length and the thickness of the chambers; if the size of the chambers is fixed, the frequency can then be regulated by inserting partitions. Moreover, as a unique merit of the origami-inspired design, the effective bandwidth of the origami window can also be effectively tuned via folding. A small folding angle always gives rise to broad 10dB TL bandwidth, while the TL peaks are slightly affected.

3.3 Optimization of the single-layer silencing window

We then discuss how to design a single-layer origami silencing window for a given target frequency band. To this end, a comprehensive numerical analysis based on FEM in COMSOL (with the same setup shown in Fig. 3(a)) is carried out to elucidate the sound attenuation characteristics of the window with different partition forms and different geometric parameters. From a practical application point of view, the geometric parameters a and w are constrained by $40\ \text{mm} \le a \le 100\ \text{mm}$ and $20\ \text{mm} \le a \le 80\ \text{mm}$ to prevent oversized or undersized design. Considering that a small folding angle gives rise to broader bandwidth of noise reduction (Figs. 4(c), (f), (k), and (n)), the folding angle is fixed to $\theta = 15^\circ$. According to the typical frequency distribution characteristics of traffic noise [39], the frequency band [300, 1500] (Hz) is focused here.

Figure 5 displays the effects of partition forms and chamber geometries on the sound attenuation performance. Four partition forms are considered, using discrete values of a and w, i.e., $a \in [40,\ 45,\ 50,...,\ 95,\ 100](\text{mm})$ and $w \in [20,\ 25,\ 30,...,\ 75,\ 80](\text{mm})$. The acoustic bands with

TL>10dB and the TL peak curves are represented by shaded areas and dashed curves, respectively. For all four partition forms, increasing the chamber side length a will always shift the TL peak toward lower frequency, and enlarging the chamber thickness w will broaden the effective bandwidth as well

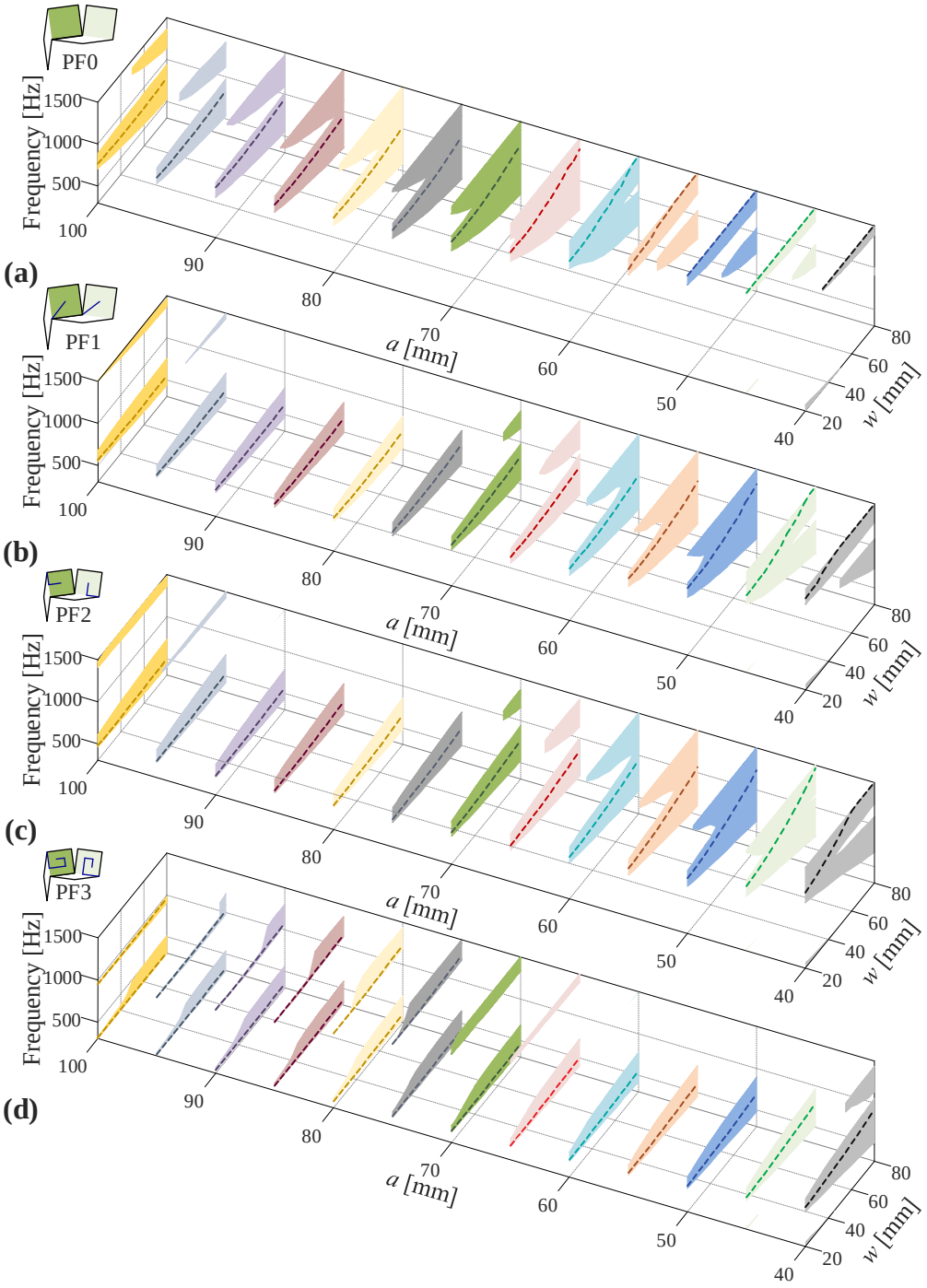

Figure 5. Acoustic characterization of the single-layer origami silencing window with different geometries and partition forms when $\theta = 15^{\circ}$. (a) PF0, (b) PF1, (c) PF2, (d) PF3. The shades denote the 10db TL stopbands, and the dashed curves denote the TL peaks.

as mildly lift the TL peak frequency. Particularly, two separate 10dB TL bands are achievable in some window designs. For the PF3 designs with a relatively large a and w, two distant TL peaks are observed.

Figure 5 also provides us with the necessary data for optimal design. In fact, by adjusting the four design parameters, the TL performance can be tuned over a wide range. For example, the TL peak can vary between 310Hz (PF3, $a=100\text{mm}, w=50\text{mm}$) and 1500 Hz (PF0, $a=60\text{mm}, w=80\text{mm}$), and the individual bandwidth can vary from 50 Hz (PF3, $a=95\text{mm}, w=20\text{mm}$) to 950 Hz (PF0, $a=85\text{mm}, w=80\text{mm}$). Hence, based on Fig. 5, we can quantitatively evaluate the sound attenuation performance for a target frequency band and then determine the optimal design via discrete optimization. In detail, the average TL of a specific window design x is employed as the objective function of optimization, which is defined as [85,96–98]:

$$F(x)=\overline{\mathrm{TL}(\Delta f)}=\frac{1}{f_u-f_l}\int_{f_l}^{f_u}W(f)\cdot\mathrm{TL}(f)\mathrm{d}f=\frac{1}{N}\sum_{i=1}^{N}W_i\cdot\mathrm{TL}_i, \tag{3}$$

where f_u, f_l represent the upper and lower bounds of the target frequency band, respectively; $i=1,2,...,N$ denotes the discrete frequency points used in the numerical simulation. Without loss of generality, all frequencies are assumed to have the same weighting $W_i=1$. Hence, the optimization problem can be formulated as

$$\max_x\ F(x)\quad\text{for}\quad x=\{x_1,x_2,...\}, \tag{4}$$

where x_i is the design candidate used in simulations as shown in Fig. 5.

As an example, with a narrow target frequency band [800, 1000] Hz, the contours of average TL for the four different partition forms are displayed in Figs. 6(a)~6(d). Through discrete optimization, the optimal design corresponding to each partition form can be determined. For PF0, $a=85$ mm, $w=75$ mm; for PF1: $a=65$ mm, $w=80$ mm, for PF2: $a=60$ mm, $w=80$ mm, and for PF3: $a=40$ mm, $w=80$ mm. With the same target frequency band, the optimal designs corresponding to different partition forms differ significantly, while their performance is relatively close and good (Fig. 6(e)). We can then choose the appropriate window design according to the actual needs and geometric constraints. Particularly, the optimal design of PF2 ($a=60$ mm, $w=80$ mm) delivers the best performance, with an average TL of 29.23dB.

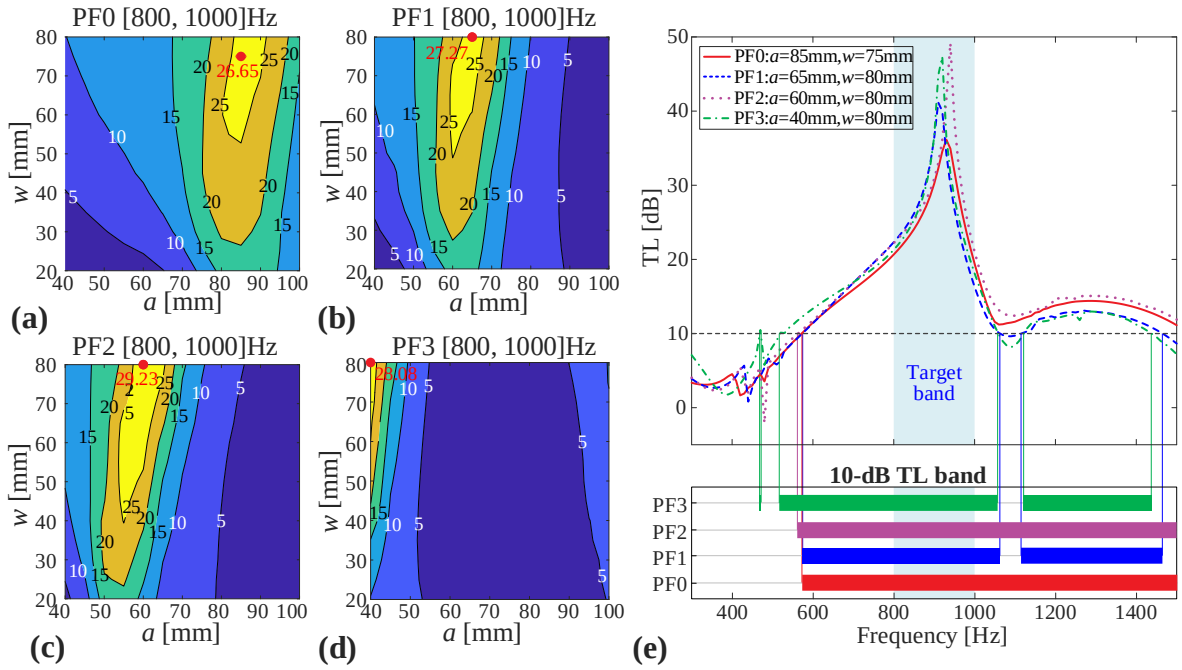

Figure 6. Optimization results for the target band [800, 1000] Hz when the folding angle $\theta = 15^{\circ}$. The distributions of the average TL with respect to the geometric parameters a and w for (a) PF0, (b) PF1, (c) PF2, (d) PF3 are displayed, in which the solid dot denote the optimal design corresponding to the maximum average TL. (e) The TL curves and the 10dB TL bands (i.e., warranting more than 90% reduction of the energy of noise) of the optimal designs for different partition forms, in which the target band is shaded.

Note that the given range of geometric parameters cannot guarantee favorable average TL performance for all given target bands. For example, if we focus on low-frequency noise reduction, say, setting [300, 500] Hz as the target frequency band, although the optimal designs corresponding to the four partition forms can still be obtained via discrete optimization (Figs. 7(a)~7(d)), their performance deteriorates seriously, except for PF3. It shows from Fig. 7(e) that with the optimal design corresponding to PF0 and PF1, only a small portion of the target band satisfies TL>10dB, and the TL peaks are far away from the target band. With the optimal design corresponding to PF2, although the peak locates at the boundary of the target band (i.e., 500 Hz), there is still an interval in which the TL values are lower than 10dB. The only acceptable one is the optimal design corresponding to PF3 (i.e., $a = 80$ mm, $w = 100$ mm), whose TL>10dB band covers the major portion of the target, and the average TL reaches 17.63dB.

Moreover, if we aim at broadband sound attenuation, e.g., setting [300, 1500] Hz as the target band, the obtained optimal designs cannot meet the requirements of full-band noise reduction (Fig. 8). Figure 8(e) indicates that with the four optimal designs corresponding to the four partition forms (Fig.

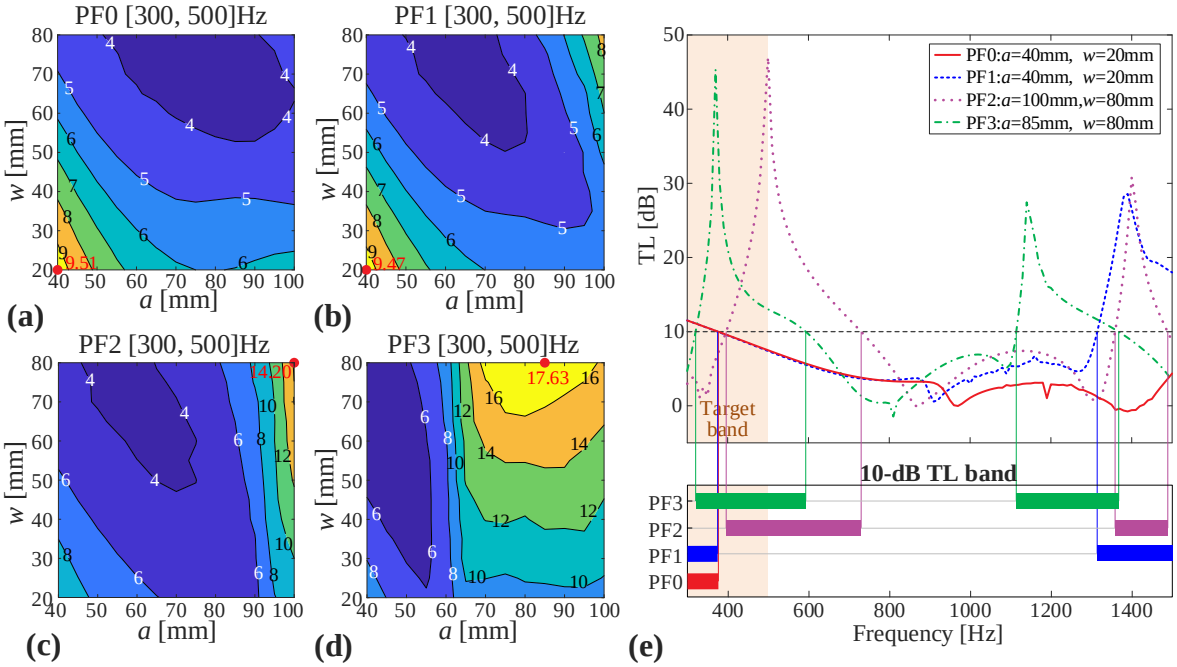

Figure 7. Optimization results for the target band [300, 500] Hz when the folding angle $\theta = 15^{\circ}$. The distributions of the average TL with respect to the geometric parameters a and w for (a) PF0, (b) PF1, (c) PF2, and (d) PF3 are displayed, in which the solid dot denotes the optimal design corresponding to the maximum average TL. (e) The TL curves and the 10dB TL bands of the optimal designs for different partition forms, in which the target band is shaded.

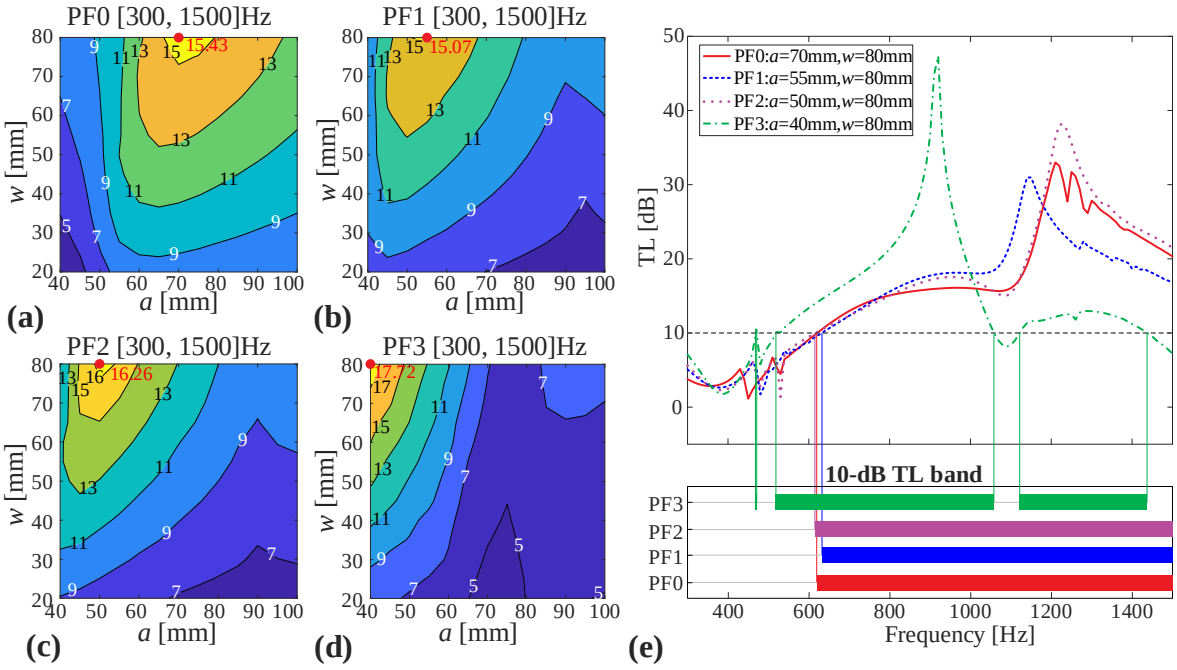

Figure 8. Optimization results for the target band [300, 1500] Hz when the folding angle $\theta = 15^{\circ}$. The distributions of the average TL with respect to the geometric parameters a and w for (a) PF0, (b) PF1, (c) PF2, (d) PF3 are displayed, in which the solid dot denote the optimal design corresponding to the maximum average TL. (e) The TL curves and the 10dB TL bands of the optimal designs for different partition forms.

8(a)~8(d)), the 10dB bands cannot cover the full band. The target band coverage ratios of the four optimal designs corresponding to PF0, PF1, PF2, and PF3 are 72.73%, 71.90%, 73.55%, and 71.07%, respectively. This, therefore, requires us to seek ways to further broaden the effective band and improve the coverage of the target band.

4 Multi-layer origami silencing window

Stacking multiple layer chambers would allow to achieve broadband sound attenuation [85]. This motivates us to make use of the origami's extensibility and explore the possibility of broadening the effective noise reduction band by cascading two geometrically compatible origami layers. Thus, instead of 'globally' re-designing a new multi-layer window, the previous parameter sweeping results on single layers (Fig. 5) will be used to guide the design toward a specific sound attenuation requirement.

Specifically, two origami layers are kinematically compatible if they share the same edge length a of the modular origami. The thickness of the two layers (w_1 and w_2) and the partition forms are designable parameters. Considering the usual wall thickness, the overall thickness of the silencing window is constrained to 240 mm, i.e., $l_1 + w_1 + l_2 + w_2 + l_3 \le 240$ mm. Since $l_1 = l_3 = 5$ mm and $l_2 = 110$ mm (Fig. 3(b)), we have

$$w_1 + w_2 \le 120 \text{ mm}. \tag{5}$$

Setting the whole band [300, 1500] Hz as the target, we first examine whether the effective bands ($\mathrm{TL} \ge 10$ dB) of two origami layers can cover the target band when superposed. The four partition forms can be combined in six different ways. For each combination, the effects of the edge length a (shared by both layers, $40 \le a \le 100$ (mm)) and the thickness of the two layers w_1 and w_2 ($20 \le w_1, w_2 \le 80$ (mm)) on the target-band coverage are examined. Figure 9 indicates that for all combinations, 100% coverage of the target band is not achievable in the whole parameter range. However, except for PF1+PF2, more than 80% coverage is possible for the other five combination

cases, and more than 95% coverage is only achievable in the PF0+PF3 combination. Hence, the PF0+PF3 combination is examined in detail. Figure 9(d) reveals that >80% coverage is achievable if the edge length is $60 \le a \le 100$ (mm). When $a = 60$ mm, >80% coverage of the target band is

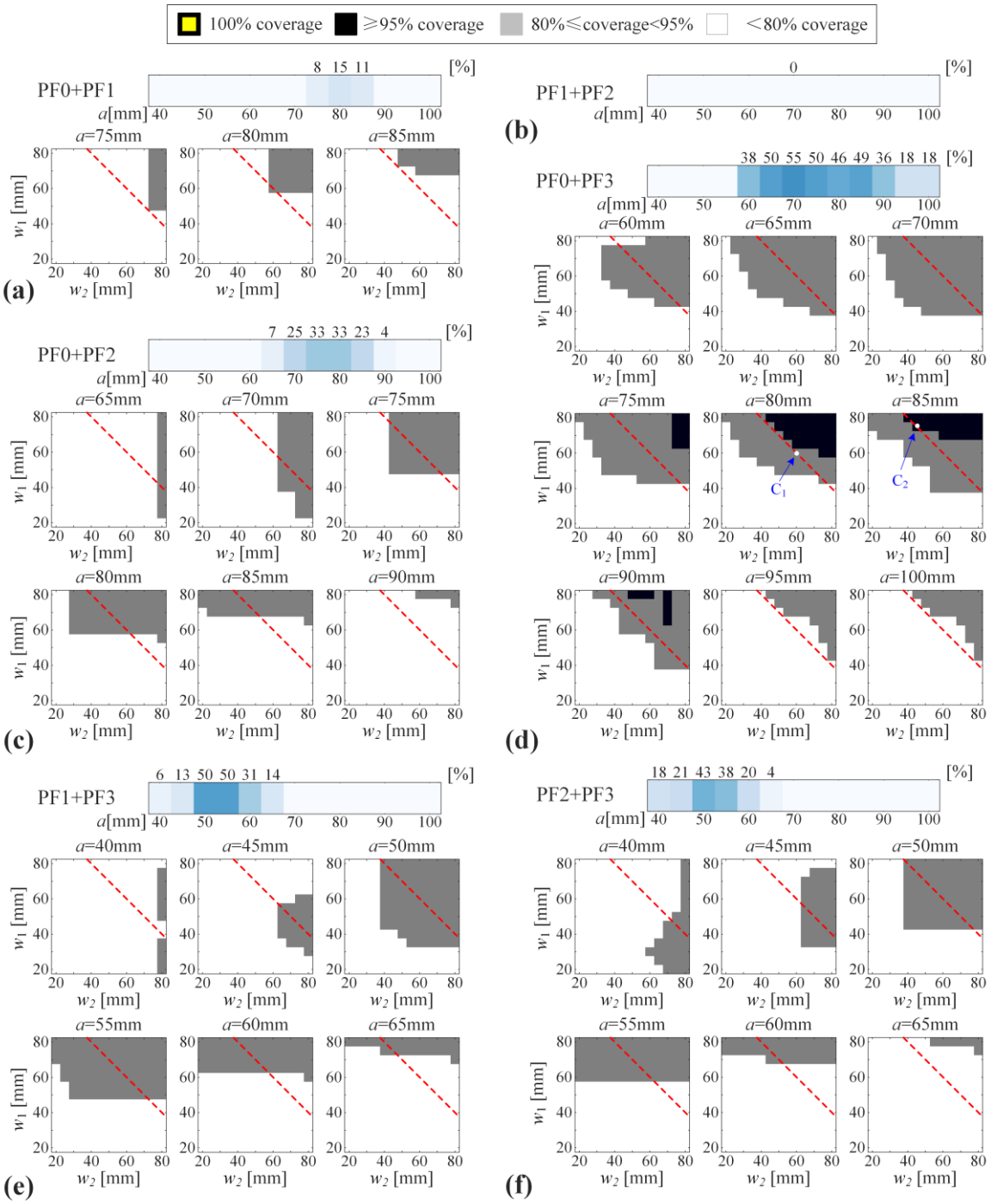

Figure 9. The coverage of the frequency band [300, 1500] Hz for different combinations of layers. (a) PF0+PF1, (b) PF1+PF2, (c) PF0+PF2, (d) PF0+PF3, (e) PF1+PF3, (f) PF2+PF3. The geometric constraint is denoted by the dashed lines in the 2D array plot. The number above the horizontal bar plot indicates the percentage of the area with more than 80% coverage of the target band in the $w_1 - w_2$ plane.

reached in the grey area, which occupies 38% of the area in the $w_1 - w_2$ plane. When a is increased to 75mm, >95% coverage is possible, but the feasible region (denoted by the black area) is beyond the constraint line $w_1 + w_2 = 120$ mm (denoted by the dashed line). When $a = 80$ mm, the area corresponds to >95% coverage is further expanded, but none of them satisfies the constraint Eq. (5). When $a = 85$ mm, parameters that meet more than 95% coverage and geometric constraint Eq. (5) are found.

Although a direct superposition of the effective bands from two single origami layers is not exactly the same as the effective band obtained by the double-layer window as a whole, Fig. 9 still provides intuitive and useful information for determining the geometric parameters of the two origami layers. By selecting parameters that fall in or are close to the >95% coverage region, we can hopefully achieve a good noise reduction for the target band [300, 1500] Hz. As a result, two groups of parameters are taken to examine the effect: point C_1 ($a = 80$, $w_1 = 60$, $w_2 = 60$ (mm)) and point C_2 ($a = 85$, $w_1 = 75$, $w_2 = 45$ (mm)) in the PF0+PF3 combination. Their positions are denoted by white dots in Fig. 9(d); C_1 locates outside but very close to the >95% region, while C_2 is inside the >95% region. Both points C_1 and C_2 satisfy the geometric constraint Eq. (5).

Figure 10 displays the TL of the two-layer origami silencing window with design parameters at point C_1 and C_2 in the PF0+PF3 combination. For reference purposes, the TL curves corresponding to the two constituent single-layer windows are also provided. It shows that with the double-layer window, the coverage of the $\mathrm{TL} \geq 10$ dB band is increased from 73.55% of a single-layer window (Fig. 8(e)) to 82.64% at point C_1 and 80.17% at point C_2, while the expected full coverage is still not achieved. By cascading the two layers, the TL peaks of the constituent layers are well exploited. However, at some frequency intervals, the double-layer window performs worse than a single-layer due to the destructive effect of the evanescent wave coupling [99]. For example, the single-layer window ($\mathrm{PF3}: a = 85\mathrm{mm}$, $w_1 = 45\mathrm{mm}$) yields >10 dB noise reduction at 500Hz, but the TL of the double-layer window with parameters C_2 is only 8.97 dB. Moreover, we note that although point C_1 locates outside the >95% region while point C_2 locates inside the >95% region, the actual coverage of the two-layer window with parameters C_1 is superior to that with parameters C_2. This, therefore, raises the demand for studying the interference between the two origami layers in our future research.

If the target band is narrowed to [500, 1200] Hz, which is typically the dominant frequency interval of the traffic noise [81], we can also re-design the two-layer window based on similar procedures used above. For this target band, all the six combinations of partition forms can give rise to >80% coverage. Particularly, we find that the PF1+PF3 combination exhibit good performance,

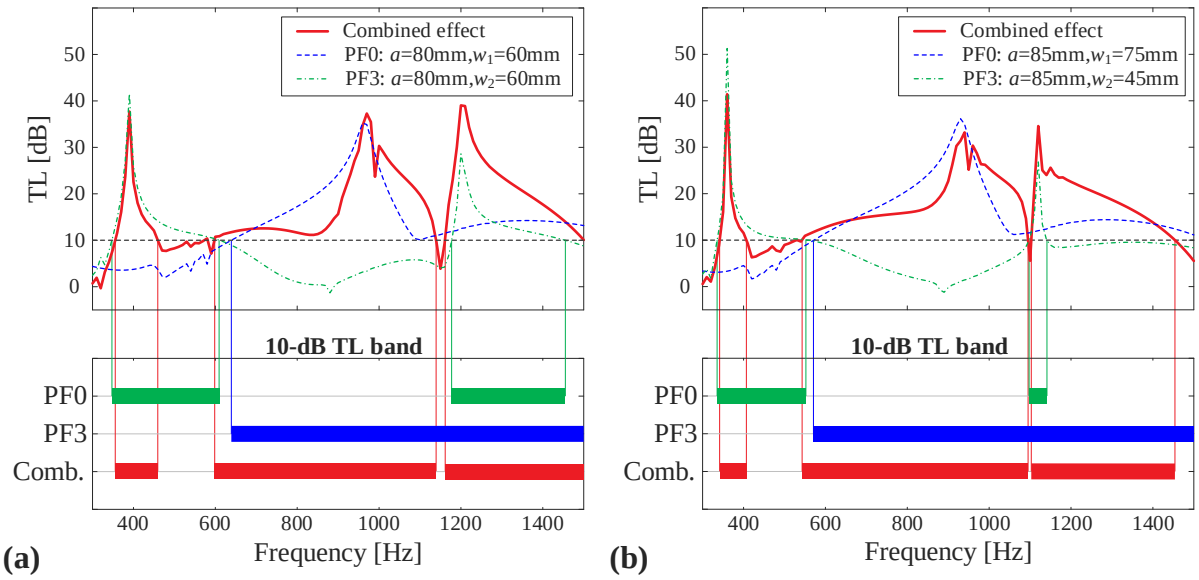

Figure 10. TL curves and 10-dB TL bands of the double-layer silencer windows. (a) Parameters C_1: $a=80,\ w_1=60,\ w_2=60$ (mm), (b) parameters C_2: $a=85,\ w_1=75,\ w_2=45$ (mm). For reference, the TL curves and bands corresponding to the constituent single layers are also plotted.

manifested by a large area of more than 80% coverage and the achievability of 100% coverage (Fig. 11(a)). Hence, the parameters that are close to or fall in the >95% (or 100%) coverage region are preferred. As an example, point C_3 ($a=60,\ w_1=60,\ w_2=60$ (mm)) in the PF1+PF3 combination is studied to exemplify the effect of the double-layer window. Figure 11(b) reveals that the 10-dB TL band fully covers the target band because the constituent single-layer windows achieve good complementarity. The double-layer window not only maintains a high TL value around the TL peaks of the constituent single-layer window but also enables a significant improvement in the regions where the constituent single-layer windows perform poorly, such as around 700 Hz and 1100 Hz.

Note that the TL band broadening achieved by stacking two origami layers is the result at a folding angle of 15°. Since the two origami layers share the same edge length a, the double-layer window can still maintain a single degree of freedom for folding. Increasing the folding angle θ, the effective

band will be narrowed due to the enlarged duct area. However, effective noise reduction can still be achieved in a low-frequency band near 500 Hz and a high-frequency band around 900~1000 Hz.

The above two examples well demonstrate the advantages acquired by incorporating two origami layers in the design of the silencing window, i.e., improved sound attenuation at a specified frequency band and broadband sound suppression. It is the unique extensibility of modular origami that allows different origami layers to be stacked without affecting the overall foldability. Therefore, if aiming at different actual requirements, rather than re-designing the whole window, noise suppression in different user-prescribed frequency bands can be achieved by simply replacing the constituent origami layers. This is also a demonstration of the programmability that origami offers [84,85]. Note that under the constraint of the wall thickness, full-band ([300, 1500] Hz) attenuation is not perfectly realized in Fig. 10. However, by further increasing the design freedom, e.g., incorporating new forms of partition inside the chambers, we are hopeful to achieve better wide-band noise reduction performance.

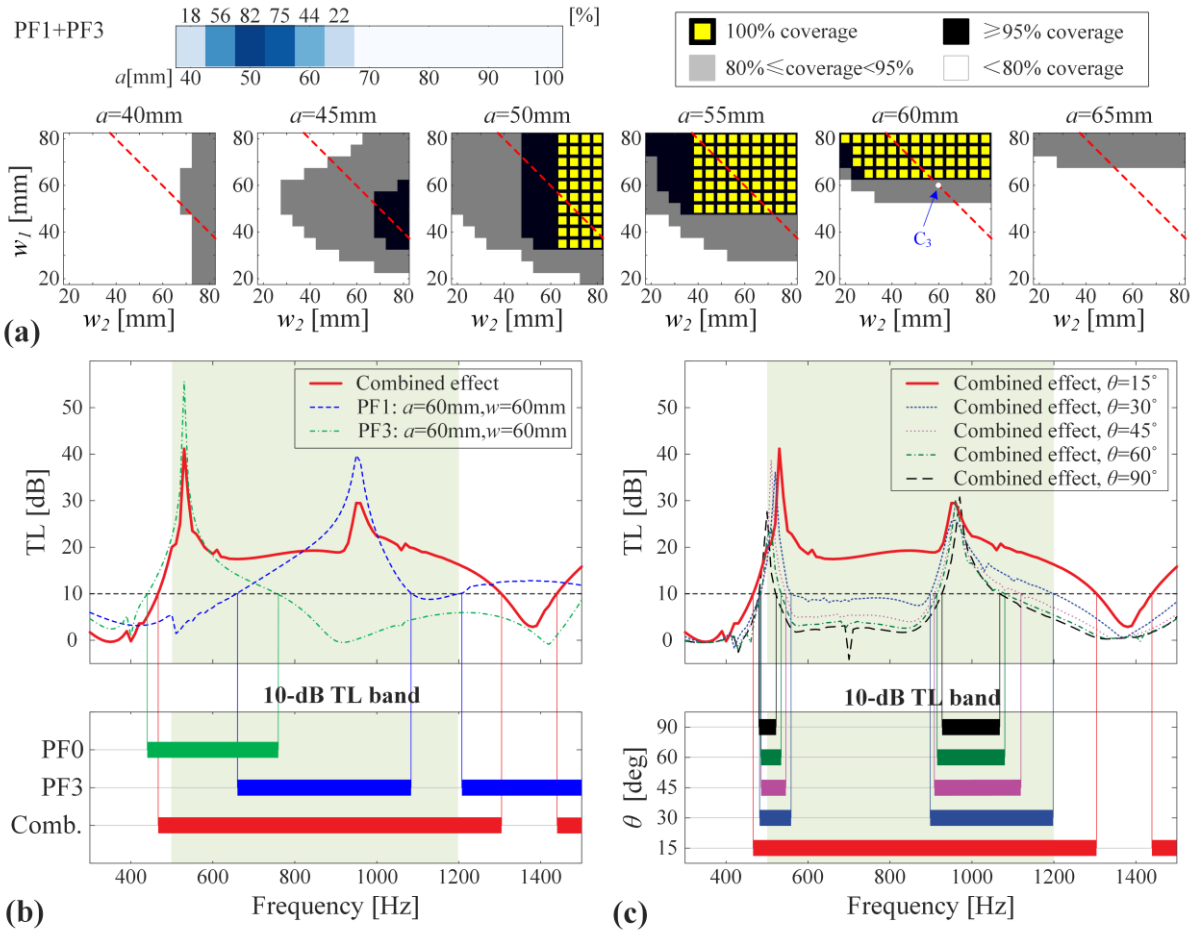

Figure 11. Performance of double-layer origami silencing window for the target band [500, 1200] Hz. (a) The coverage of the target frequency band [500, 1200] Hz for the PF1+PF3 combination. (b)TL curves

and 10-dB TL bands of the double-layer silencer window with parameters at point C_3. For reference, the TL curves and bands corresponding to the constituent single layers are also plotted. (c) TL curves and 10-dB TL bands of the double-layer origami silencing window when the folding angle θ is 15°, 30°, 45°, 60°, and 90°.

5 Tunable ventilation performance

Building upon the above-mentioned adjustable noise reduction, we continue to analyze the adjustable ventilation performance brought by the origami foldability with an attempt to achieve a balance between the originally contradictory noise reduction and air ventilation. To evaluate the ventilation effect and the indoor air quality, the Local Mean Age of air (LMA) at a particular location P of a ventilated domain, defined as the average time that is needed for the molecules of air to reach that location since they enter the room [100,101], is examined. LMA is evaluated through Computational Fluid Dynamic (CFD) simulations.

In this research, a single dormitory ($2.43\text{m}\times2.72\text{m}\times2.67\text{m}$) at the Fudan University is studied using the commercial simulation software ANSYS 19.0. Figure 12 displays the CFD model of the room to be ventilated. The room is discretized into free-tetrahedral elements, with the maximum distance between nodes of 0.236 m and the minimum distance of 2.36×10^{-3} m. For comparison purposes, two cases are studied. In the first case, the origami silencing window shown in Figure 11 (PF1+PF3combination, $a=60$ mm and $w=60$ mm for both layers) is used. In the second case, a conventional sliding window is considered. The parameter x is taken from (0.297, 0.287, 0.257, 0.21, 0.148, 0.077) m so that the sliding window share the same opening area with the origami window at folding angles of (90, 75, 60, 45, 30, 15) degree. The air blows towards the window and exits through the open door. During the calculations, the airflow is considered as steady, incompressible and turbulent. The k-ε turbulence model [102] is adopted to simulate the main flow turbulence far from the

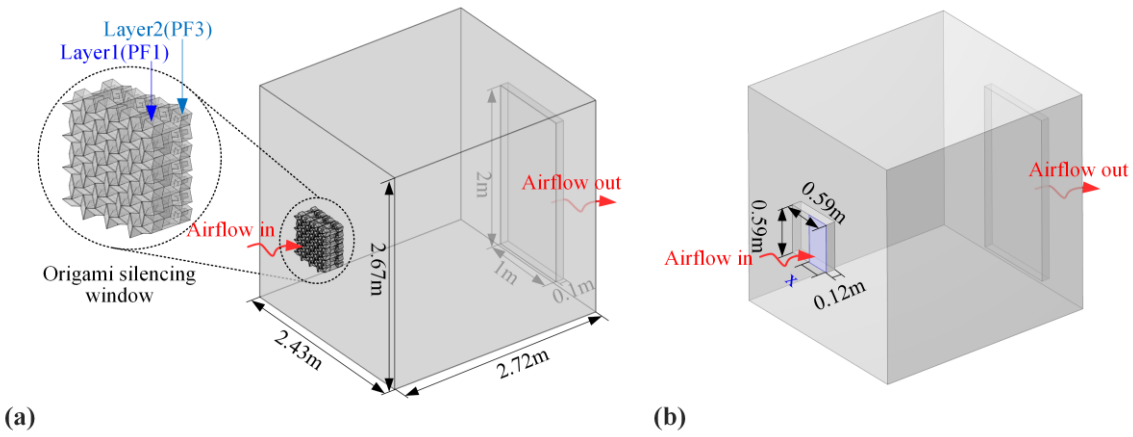

Figure 12. The CFD models of the ventilated room with different windows. (a) The room with the origami silencing window. (b) The room with a conventional sliding window, where the opening is denoted by blue, and its dimension is controlled by the parameter *x*.

smooth walls, and standard wall function is applied. The SIMPLE algorithm with a second order scheme for the convective terms is used for coupling the pressure and velocity [102]. In the inlet area, an air velocity of 1 m/s, an air temperature of 300K, and an air density of $1.225\ \mathrm{kg/m^3}$ are specified.

Figure 13(a) displays the distributions of the LMA in the vertical section of the room when the origami window is folded to 15°, 30°, 45°, 60°, 75°, and 90°. It reveals that with the increase of the folding angle θ, LMA reduces substantially over the whole room. To quantify the Age of Air (AoA) level of the overall room, in addition to the LAM distributions, we further evaluate the average AoA within the whole domain, defined as [100]:

$$\bar{\tau} = \frac{\int_{\mathrm{Vol}} \tau_P \mathrm{d}x\mathrm{d}y\mathrm{d}z}{\mathrm{Vol}}, \tag{6}$$

where τ_P is the LMA at any point P within the domain. For the origami window, the evolution of the average AOA $\bar{\tau}$ and the average TL over the target band [500, 1200] Hz with respect to the folding angle θ are plotted in Fig. 13(b) and Fig. 13(c), respectively (dash-dot curves). Benefiting from the foldability of the origami silencing window, the noise reduction and air ventilation are well balanced, and they can be effectively and conveniently adjusted according to requirements. For example, during the daytime, especially during rush hours, traffic noise become significant [41]. To effectively reduce the noise, we can fold the origami window to $15\sim30^\circ$ so that the incoming traffic noise of 500~1200 Hz can be effectively suppressed, resulting in an average TL of more than 10dB, that is, a more than 90% reduction of noise. The insulation of noise will not impede the air ventilation. Despite the small

ventilation area, the origami window can still ensure a certain amount of air ventilation, with the average AoA within the room maintained between 200 s and 450 s. At night, especially during late night sleeping hours, traffic noise becomes weaker [41]. To improve the sleep quality [35], we can fold the origami window to $75 \sim 90^{\circ}$ to enhance the ventilation performance of the room, with the average AoA of the room reduced to below 130 s. Due to the presence of resonant chambers, the origami window could still maintain a noise reduction of more than 7dB despite the increased ventilation area.

Compared with the conventional sliding window (dotted curves in Fig. 13(b) and 13(c)), when the opening area is relatively large (i.e., with large folding angle θ), the ventilation performances of the two windows are similar. With reduced folding angle θ, the ventilation performances of both windows are weakened, and the average AoA of the origami window is larger than that of the sliding window. This is because when the folding angle is small, the duct of the origami window has a small cross-section area, which would generate a large airflow resistance [78,103]. On the other hand, in terms of the silencing performance, the average TL of the origami windows significantly outperforms the conventional sliding window. Even with a relatively small ventilation area, the sliding window cannot insulate noise effectively (TL<8dB), while the origami window can achieve effective noise reduction with a high TL level. The above examples and the comparison between the origami window and the conventional sliding window fully showcase the unique benefits of the modular origami window design, including the extraordinary adjustability, functional balance between noise reduction and air ventilation, and ultimately enhanced human comfort.

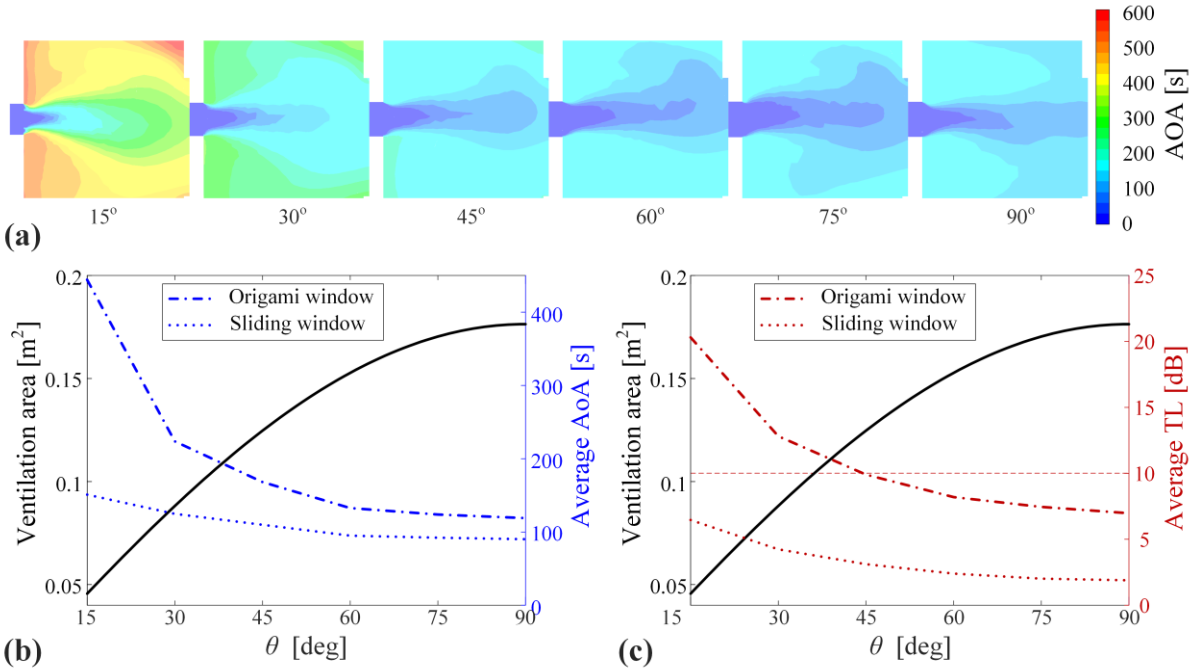

Figure 13. Performance of air ventilation and noise reduction. (a) LMA distribution in the vertical section of the room; (b) Evolution of the ventilation area and the average AoA with respect to the folding angle. (c) Evolution of the ventilation area and the average TL with respect to the folding angle.

6. Summary and Conclusions

To solve the dilemma between the natural ventilation and noise mitigation, a novel reconfigurable silencing window based on modular origami structures is proposed in this study. The opening area of the origami window was tuned by a single-degree-of-freedom folding mechanism. Comprehensive FE simulations were conducted to determine the acoustic characteristics of the proposed window, as well as the design flexibility and tuning ability arising from the modular origami concept. CFD simulations were also conducted to evaluate the air exchange rate of the proposed origami window at different folding angles, and the holistic performance with both acoustic and ventilation considerations was compared to that of a conventional sliding window. Specifically, the design merits are demonstrated in three aspects: (1) Based on a single-DOF folding mechanism, the area of the ducts and the area ratio between the chambers and the ducts would change significantly, which therefore allows the effective tuning of the sound attenuation bandwidth and the ventilation effect. (2) The geometry and the internal partitions of the chambers are designable in a large space, which significantly enriches the frequency characteristics of the TL profile of a single origami layer. (3) Aiming at noise reduction in the target frequency band, discrete numerical optimization could

determine the optimal design corresponding to the maximum average TL; for the demand of broadband noise reduction, multiple layers can be selected and stacked according to the effective band characteristics of a single layer. The novel origami-inspired design, in addition to achieving a balanced ventilation and noise reduction, overcomes many existing problems in silencing windows by exploiting the foldability and extensibility of the modular origami, e.g., acoustics and ventilation tunability, design flexibility, and adaptability to different working scenarios.

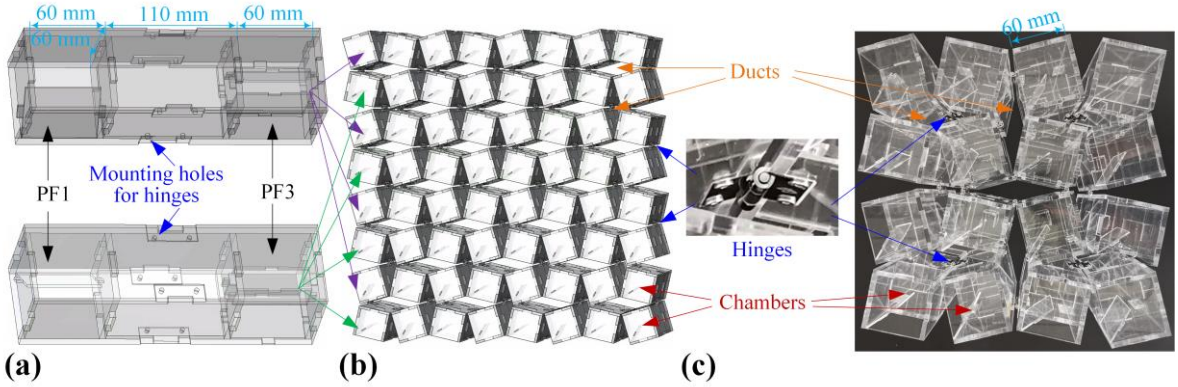

Figure 14. Proof-of-concept design and prototype of the origami silencing window. (a) CAD sign of the constituent modules, in which the first layer is of PF1, and the second layer is of PF3; (b) CAD design of a dual-layer 7×7 origami silencing window; (c) proof-of-concept prototype of a dual-layer 3×3 origami silencing window. The hinge for connecting and folding is shown in an enlarged view.

It is worth mentioning that there still exist several problems awaiting solutions in terms of practical applications. For example, mechanisms are needed to connect the irregularly shaped origami window to the wall, to deal with the changes in the gaps between the window and the wall after folding reconfiguration, and to achieve automatic folding. At this stage, experimental verification of the proposed window design has not been carried out yet, which will be our future endeavor. This research aims at demonstrating the design principles, feasibility and flexibility first, and the prototype in Fig. 14 can be considered as a proof-of-concept. The geometry and partition form of the design is consistent with those in Fig. 11. Basically, a 7×7 dual-layer window can be constructed based on two constituent modules (Fig. 11(a) and 11(b)), with the first layer of PF1 and the second layer of PF3. Mounting holes are reserved for hinges, which are used for connecting and folding. Figure 11(c) shows the photo of a 3×3 dual-layer window prototype.

Overall, this research synthesizes the folding kinematics of modular origami and acoustic resonances to yield a novel origami silencing window for the balance and tunability of noise reduction

and air ventilation. The extraordinary designability, reconfigurability, optimizability, and extensibility of the origami solution uncovered in this research will provide a new avenue for the design and development of planar acoustic devices.

CRediT authorship contribution statement

Xiaomeng Jin: Writing – original draft, Methodology, Investigation, Formal Analyais, Visualization. **Hongbin Fang**: Writing – review & editing, Conceptualization, Validation, Visualization, Supervision, Project administration, Funding acquisition. **Xiang Yu**: Writing – review & editing, Software, Supervision. **Jian Xu**: Writing – review & editing, Resources, Supervision. **Li Cheng**: Writing – review & editing, Conceptualization, Supervision.

Declaration of competing interest

The authors declare that they have no known competing financial interests or personal relationships that could have appeared to influence the work reported in this paper.

Acknowledgment.

This research was supported by the National Natural Science Foundation of China (Grant No. 11902078) and the Shanghai Rising Star Program (Grant No. 20QA1400800). The authors would like to thank Zihan He, Wen Zhang, Rui Shi, and Zi'an Zhang for their assistance in 3D modeling and CFD simulations.

Reference

[1] A. Muzet, Environmental noise, sleep and health, Sleep Med. Rev. 11 (2007) 135–142. https://doi.org/10.1016/j.smrv.2006.09.001.

[2] F.F. Zacarías, R.H. Molina, J.L.C. Ancela, S.L. López, A.A. Ojembarrena, Noise exposure in preterm infants treated with respiratory support using neonatal helmets, Acta Acust. United with Acust. 99 (2013) 590–597. https://doi.org/10.3813/AAA.918638.

[3] F. Minichilli, F. Gorini, E. Ascari, F. Bianchi, A. Coi, L. Fredianelli, G. Licitra, F. Manzoli, L. Mezzasalma, L. Cori, Annoyance judgment and measurements of environmental noise: A focus on italian secondary schools, Int. J. Environ. Res. Public Health. 15 (2018). https://doi.org/10.3390/ijerph15020208.

[4] L.C. Erickson, R.S. Newman, Influences of background noise on infants and children, Curr. Dir. Psychol. Sci. 26 (2017) 451–457. https://doi.org/10.1177/0963721417709087.

[5] W.K. Chung, C.K. Chau, M. Masullo, A. Pascale, Modelling perceived oppressiveness and noise annoyance responses to window views of densely packed residential high-rise environments, Build. Environ. 157 (2019) 127–138. https://doi.org/10.1016/j.buildenv.2019.04.042.

[6] E. Öhrström, A. Skånberg, H. Svensson, A. Gidlöf-Gunnarsson, Effects of road traffic noise and the benefit of access to quietness, J. Sound Vib. 295 (2006) 40–59. https://doi.org/10.1016/j.jsv.2005.11.034.
[7] L. Vukić, V. Mihanović, L. Fredianelli, V. Plazibat, Seafarers' perception and attitudes towards noise emission on board ships, Int. J. Environ. Res. Public Health. 18 (2021). https://doi.org/10.3390/ijerph18126671.
[8] L. Rossi, A. Prato, L. Lesina, A. Schiavi, Effects of low-frequency noise on human cognitive performances in laboratory, Build. Acoust. 25 (2018) 17–33. https://doi.org/10.1177/1351010X18756800.
[9] H.M.E. Miedema, C.G.M. Oudshoorn, Annoyance from transportation noise: Relationships with exposure metrics DNL and DENL and their confidence intervals, Environ. Health Perspect. 109 (2001) 409–416. https://doi.org/10.1289/ehp.01109409.
[10] G. Licitra, L. Fredianelli, D. Petri, M.A. Vigotti, Annoyance evaluation due to overall railway noise and vibration in Pisa urban areas, Sci. Total Environ. 568 (2016) 1315–1325. https://doi.org/10.1016/j.scitotenv.2015.11.071.
[11] J. Dratva, H.C. Phuleria, M. Foraster, J.M. Gaspoz, D. Keidel, N. Künzli, L.J. Sally Liu, M. Pons, E. Zemp, M.W. Gerbase, C. Schindler, Transportation noise and blood pressure in a population-based sample of adults, Environ. Health Perspect. 120 (2012) 50–55. https://doi.org/10.1289/ehp.1103448.
[12] W. Babisch, B. Beule, M. Schust, N. Kersten, H. Ising, Traffic noise and risk of myocardial infarction, Epidemiology. 16 (2005) 33–40. https://doi.org/10.1097/01.ede.0000147104.84424.24.
[13] D. Petri, G. Licitra, M.A. Vigotti, L. Fredianelli, Effects of exposure to road, railway, airport and recreational noise on blood pressure and hypertension, Int. J. Environ. Res. Public Health. 18 (2021). https://doi.org/10.3390/ijerph18179145.
[14] J.L. Cueto, A.M. Petrovici, R. Hernández, F. Fernández, Analysis of the impact of bus signal priority on urban noise, Acta Acust. United with Acust. 103 (2017) 561–573.
[15] L. Fredianelli, S. Carpita, M. Bernardini, L.G. Del Pizzo, F. Brocchi, F. Bianco, G. Licitra, Traffic Flow Detection Using Camera Images and Machine Learning Methods in ITS for Noise Map and Action Plan Optimization, Sensors. 22 (2022). https://doi.org/10.3390/s22051929.
[16] A. Ruiz-Padillo, D.P. Ruiz, A.J. Torija, Á. Ramos-Ridao, Selection of suitable alternatives to reduce the environmental impact of road traffic noise using a fuzzy multi-criteria decision model, Environ. Impact Assess. Rev. 61 (2016) 8–18. https://doi.org/10.1016/j.eiar.2016.06.003.
[17] F. Bunn, P.H.T. Zannin, Assessment of railway noise in an urban setting, Appl. Acoust. 104 (2016) 16–23. https://doi.org/10.1016/j.apacoust.2015.10.025.
[18] C. Iglesias-Merchan, L. Diaz-Balteiro, M. Soliño, Transportation planning and quiet natural areas preservation: Aircraft overflights noise assessment in a National Park, Transp. Res. Part D Transp. Environ. 41 (2015) 1–12. https://doi.org/10.1016/j.trd.2015.09.006.
[19] P. Gagliardi, L. Teti, G. Licitra, A statistical evaluation on flight operational characteristics affecting aircraft noise during take-off, Appl. Acoust. 134 (2018) 8–15. https://doi.org/10.1016/j.apacoust.2017.12.024.
[20] X. Yan, H. Song, Z. Peng, H. Kong, Y. Cheng, L. Han, Review of Research Results concerning the Modelling of Shipping Noise, Polish Marit. Res. 28 (2021) 102–115. https://doi.org/10.2478/pomr-2021-0027.
[21] E. Murphy, E.A. King, An assessment of residential exposure to environmental noise at a shipping port, Environ. Int. 63 (2014) 207–215. https://doi.org/10.1016/j.envint.2013.11.001.
[22] L. Fredianelli, T. Gaggero, M. Bolognese, D. Borelli, F. Fidecaro, C. Schenone, G. Licitra, Source characterization guidelines for noise mapping of port areas, Heliyon. 8 (2022) e09021. https://doi.org/10.1016/j.heliyon.2022.e09021.
[23] M. Nastasi, L. Fredianelli, M. Bernardini, L. Teti, F. Fidecaro, G. Licitra, Parameters affecting noise emitted by ships moving in port areas, Sustain. 12 (2020) 1–17. https://doi.org/10.3390/su12208742.
[24] L. Sangiuliano, B. Reff, J. Palandri, F. Wolf-Monheim, B. Pluymers, E. Deckers, W. Desmet, C. Claeys, Low frequency tyre noise mitigation in a vehicle using metal 3D printed resonant metamaterials, Mech. Syst. Signal Process. 179 (2022) 109335. https://doi.org/10.1016/j.ymssp.2022.109335.
[25] M. Ayala Botto, J.M.C. Sousa, J.M.G. Sá da Costa, Intelligent active noise control applied to a laboratory railway coach model, Control Eng. Pract. 13 (2005) 473–484. https://doi.org/10.1016/j.conengprac.2004.04.009.
[26] R. Serré, N. Gourdain, T. Jardin, M.C. Jacob, J.M. Moschetta, Towards silent micro-air vehicles: optimization of a low Reynolds number rotor in hover, Int. J. Aeroacoustics. 18 (2019) 690–710. https://doi.org/10.1177/1475472X19890260.
[27] Y. Shi, T. Li, X. He, L. Dong, G. Xu, Helicopter rotor thickness noise control using unsteady force excitation, Appl. Sci. 9 (2019). https://doi.org/10.3390/app9071351.
[28] L. Liao, Y. Zuo, H. Meng, X. Liao, Research on the technology of noise reduction in hybrid electric vehicle with composite materials, Adv. Mech. Eng. 10 (2018) 1–8. https://doi.org/10.1177/1687814018766916.
[29] B. Li, S. Guo, X. Mao, B. Cai, B. Wang, Characteristic analysis and experimental study of double layer vibration isolation device, IOP Conf. Ser. Mater. Sci. Eng. 563 (2019). https://doi.org/10.1088/1757-899X/563/3/032037.

[30] Y. Zhu, F. Bai, J. Sun, Multi-objective optimization algorithm for optimizing NVH performance of electric vehicle permanent agnet synchronous motors, J. Power Electron. (2022). https://doi.org/10.1007/s43236-022-00519-6.
[31] K. Lou, P. Xiao, A. Kang, Z. Wu, X. Dong, Effects of asphalt pavement characteristics on traffic noise reduction in different frequencies, Transp. Res. Part D Transp. Environ. 106 (2022) 103259. https://doi.org/10.1016/j.trd.2022.103259.
[32] S. Sun, J. Yang, T. Yildirim, D. Ning, X. Zhu, H. Du, S. Zhang, M. Nakano, W. Li, A magnetorheological elastomer rail damper for wideband attenuation of rail noise and vibration, J. Intell. Mater. Syst. Struct. 31 (2020) 220–228. https://doi.org/10.1177/1045389X19873406.
[33] G. Fusaro, X. Yu, J. Kang, F. Cui, Development of metacage for noise control and natural ventilation in a window system, Appl. Acoust. 170 (2020). https://doi.org/10.1016/j.apacoust.2020.107510.
[34] UK Space Management and Group, UK Higher Education Space Management Project Review of space norms, 2006. http://www.smg.ac.uk/documents/FutureChangesInHE.pdf.
[35] X. Xu, L. Lan, J. Shen, Y. Sun, Z. Lian, Five hypotheses concerned with bedroom environment and sleep quality: A questionnaire survey in Shanghai city, China, Build. Environ. 205 (2021) 108252. https://doi.org/10.1016/j.buildenv.2021.108252.
[36] X. Yang, Y. Wang, R. Zhang, Y. Zhang, Physical and Psychoacoustic Characteristics of Typical Noise on Construction Site : " How Does Noise Impact Construction Workers ' Experience ?", 12 (2021) 1–13. https://doi.org/10.3389/fpsyg.2021.707868.
[37] H.P. Lee, Z. Wang, K.M. Lim, Assessment of noise from equipment and processes at construction sites, Build. Acoust. 24 (2016) 21–34. https://doi.org/10.1177/1351010X16678218.
[38] T.W.A. Ogle, R.L. Wayson, W. Lindeman, Effect of Vehicle Speed on Sound, Transp. Res. Rec. January 01 (1991) 14–25. https://doi.org/10.1177/0361198196155900103.
[39] A. Can, L. Leclercq, J. Lelong, D. Botteldooren, Traffic noise spectrum analysis : Dynamic modeling vs . experimental observations, Appl. Acoust. 71 (2010) 764–770. https://doi.org/10.1016/j.apacoust.2010.04.002.
[40] J.L. Rochat, R. Darlene, Highway Traffic Noise, Acoust. Today. 12 (2016) 38–47.
[41] T. Gjestland, Background noise levels in Europe, 2008. http://hdl.handle.net/11250/2389006.
[42] Guoqing Zhai, B. Zhang, The Dsign of Ventilation and Sound Insulation Window, Noise Vib. Control. 34 (2004) 45-46,48. https://doi.org/1006-1355(2004)24:1<45:TFGSCD>2.0.TX;2-T.
[43] Z. Jie, X.I.E. Zhuwei, T. Yajun, L.U. Jun, Performance analysis of a new sound insulation ventilation device, J. Harbin Inst. Technol. 52 (2020) 195–200. https://doi.org/10.11918/201901053.
[44] R.D. Ford, G. Kerry, The sound insulation of partially open double glazing, Appl. Acoust. 6 (1973) 57–72. https://doi.org/10.1016/0003-682X(73)90029-7.
[45] L.S. Søndergaard, S.V. Legarth, Investigation of sound insulation for a supply air window -field measurements and occupantresponse, in: Proc. 43rd Int. Congr. Expo. Noise Control Eng. Melbourne, Aust., 2014: pp. 16–19.
[46] E. Bajraktari, J. Lechleitner, A. Mahdavi, Estimating the sound insulation of double facades with openings for natural ventilation, Energy Procedia. 78 (2015) 140–145. https://doi.org/10.1016/j.egypro.2015.11.129.
[47] Y.G. Tong, S.K. Tang, J. Kang, A. Fung, M.K.L. Yeung, Full scale field study of sound transmission across plenum windows, Appl. Acoust. 89 (2015) 244–253. https://doi.org/10.1016/j.apacoust.2014.10.003.
[48] L. Du, S.K. Lau, S.E. Lee, M.K. Danzer, Experimental study on noise reduction and ventilation performances of sound-proofed ventilation window, Build. Environ. 181 (2020) 107105. https://doi.org/10.1016/j.buildenv.2020.107105.
[49] X. Li, S.K. Tang, S.Y.C. Yim, R.Y.C. Lee, T. Hung, Noise reduction of plenum windows on the façade of a high-rise residential building next to heavy road traffic, Build. Environ. 186 (2020) 107353. https://doi.org/10.1016/j.buildenv.2020.107353.
[50] X. Yu, S.K. Lau, L. Cheng, F. Cui, A numerical investigation on the sound insulation of ventilation windows, Appl. Acoust. 117 (2017) 113–121. https://doi.org/10.1016/j.apacoust.2016.11.006.
[51] L. Du, S. Lau, S.E. Lee, Experimental Study on Sound Insulation of Ventilation Partitions, J. Acoust. 1 (2019). https://doi.org/10.20900/joa20190005.
[52] J. Kang, M.W. Brocklesby, Feasibility of applying micro-perforated absorbers in acoustic window systems, Appl. Acoust. 66 (2005) 669–689. https://doi.org/10.1016/j.apacoust.2004.06.011.
[53] X. Li, S.K. Tang, Sound insulation of plenum windows installed with rigid cylinder array, in: INTER-NOISE NOISE-CON Congr. Conf. Proc., Institute of Noise Control Engineering, 2019: pp. 1103–1109.
[54] S.K. Tang, Reduction of sound transmission across plenum windows by incorporating an array of rigid cylinders, J. Sound Vib. 415 (2018) 25–40. https://doi.org/10.1016/j.jsv.2017.11.027.
[55] T. Shimizu, S. Koizumi, Study of the compatibility between sound insulation performance and ventilation performance in gaps by installing nonwoven fabrics, Build. Environ. 94 (2015) 335–343. https://doi.org/10.1016/j.buildenv.2015.08.020.

[56] H. Huang, X. Qiu, J. Kang, Active noise attenuation in ventilation windows, J. Acoust. Soc. Am. 130 (2011) 176–188. https://doi.org/10.1121/1.3596457.
[57] B. Lam, W.S. Gan, D.Y. Shi, M. Nishimura, S. Elliott, Ten questions concerning active noise control in the built environment, Build. Environ. 200 (2021) 107928. https://doi.org/10.1016/j.buildenv.2021.107928.
[58] B. Kwon, Y. Park, Interior noise control with an active window system, Appl. Acoust. 74 (2013) 647–652. https://doi.org/10.1016/j.apacoust.2012.11.005.
[59] B. Lam, D. Shi, W.S. Gan, S.J. Elliott, M. Nishimura, Active control of broadband sound through the open aperture of a full-sized domestic window, Sci. Rep. 10 (2020) 1–7. https://doi.org/10.1038/s41598-020-66563-z.
[60] B. Lam, D. Shi, V. Belyi, S. Wen, W. Gan, K. Li, I. Lee, Active Control of Low-Frequency Noise through a Single Top-Hung Window in a Full-Sized Room, Appl. Sci. 10 (2020) 6817. https://doi.org/10.3390/app10196817.
[61] B. Lam, C. Shi, D. Shi, W.-S. Gan, Active control of sound through full-sized open windows, Build. Environ. 141 (2018) 16–27. https://doi.org/10.1016/j.buildenv.2018.05.042.
[62] T. MURAO, M. NISHIMURA, Basic Study on Active Acoustic Shielding, J. Environ. Eng. 7 (2012) 76–91. https://doi.org/10.1299/jee.7.76.
[63] S.K. Tang, A review on natural ventilation-enabling façade noise control devices for congested high-rise cities, Appl. Sci. 7 (2017). https://doi.org/10.3390/app7020175.
[64] Y. Nishimura, H. Nguyen, S. Nishimura, T. Nishimura, T. Yano, The Acoustic Design of Soundproofing Doors and Windows, Open Acoust. J. 3 (2010) 30–37. https://doi.org/10.2174/1874837601003010030.
[65] H. Nguyen, T. Yusuke, N. Yuya, N. Sohei, N. Tsuyoshi, Y. Takashi, Prediction and Experimental Study of the Acoustic Soundproofing Windows Using a Parallelepiped SVU, Open Acoust. J. 5 (2012) 8–15. https://doi.org/10.2174/1874837601205010008.
[66] S.H. Kim, S.H. Lee, Air transparent soundproof window, AIP Adv. 4 (2014) 1–8. https://doi.org/10.1063/1.4902155.
[67] X. Yu, Z. Lu, L. Cheng, F. Cui, On the sound insulation of acoustic metasurface using a sub-structuring approach, J. Sound Vib. 401 (2017) 190–203. https://doi.org/10.1016/j.jsv.2017.04.042.
[68] R. Ghaffarivardavagh, J. Nikolajczyk, S. Anderson, X. Zhang, Ultra-open acoustic metamaterial silencer based on Fano-like interference, Phys. Rev. B. 99 (2019) 024302. https://doi.org/10.1103/PhysRevB.99.024302.
[69] M. Sun, X. Fang, D. Mao, X. Wang, Y. Li, Broadband Acoustic Ventilation Barriers, Phys. Rev. Appl. 13 (2020) 044028. https://doi.org/10.1103/PhysRevApplied.13.044028.
[70] C. Shen, Y. Xie, J. Li, S.A. Cummer, Y. Jing, Acoustic metacages for sound shielding with steady air flow, J. Appl. Phys. 123 (2018) 124501. https://doi.org/10.1063/1.5009441.
[71] N. Jiménez, V. Romero-García, V. Pagneux, J.P. Groby, Rainbow-trapping absorbers: Broadband, perfect and asymmetric sound absorption by subwavelength panels for transmission problems, Sci. Rep. 7 (2017) 13595. https://doi.org/10.1038/s41598-017-13706-4.
[72] K.S. Won, J. Choe, Transmission loss analysis in a partitioned duct with porous boundaries based on combination of FEM and measurement of sound absorption coefficients, Appl. Acoust. 165 (2020) 107291. https://doi.org/10.1016/j.apacoust.2020.107291.
[73] N. Guenfoud, C. Droz, M.N. Ichchou, O. Bareille, E. Deckers, W. Desmet, On the multi-scale vibroacoustic behavior of multi-layer rectangular core topology systems, Mech. Syst. Signal Process. 143 (2020) 106629. https://doi.org/10.1016/j.ymssp.2020.106629.
[74] J.W. Jung, J.E. Kim, J.W. Lee, Acoustic metamaterial panel for both fluid passage and broadband soundproofing in the audible frequency range, Appl. Phys. Lett. 112 (2018) 041903. https://doi.org/10.1063/1.5004605.
[75] J. Mei, G. Ma, M. Yang, Z. Yang, W. Wen, P. Sheng, Dark acoustic metamaterials as super absorbers for low-frequency sound, Nat. Commun. 3 (2012) 756. https://doi.org/10.1038/ncomms1758.
[76] G. FUSARO, X. YU, F. CUI, J. KANG, Development of a metamaterial for acoustic and architectonical improvement of window design, in: Proc. 23rd Int. Congr. Acoust., Aachen, Germany, 2019. https://doi.org/10.18154/RWTH-CONV-239567.
[77] G. Fusaro, X. Yu, F. Cui, J. Kang, Development of a window system with acoustic metamaterial for air and noise control, in: Proc. 10th Int. Conf. Comput. Methods, Singapore, 2019.
[78] G. Fusaro, X. Yu, Z. Lu, F. Cui, J. Kang, A metawindow with optimised acoustic and ventilation performance, Appl. Sci. 11 (2021). https://doi.org/10.3390/app11073168.
[79] G. Fusaro, X. Yu, F. Cui, J. Kang, Full-scale metamaterial window for building application, in: Proc. 2020 Int. Congr. Noise Control Eng. INTER-NOISE 2020, Seoul, 2020.
[80] M. Thota, S. Li, K.W. Wang, Origami Metastructures for Tunable Wave Propagation, (2016). https://doi.org/10.1115/SMASIS2016-9186.
[81] M. Thota, K.W. Wang, Reconfigurable origami sonic barriers with tunable bandgaps for traffic noise mitigation, J. Appl. Phys. 122 (2017) 154091. https://doi.org/10.1063/1.4991026.

[82] M. Thota, K.W. Wang, Tunable waveguiding in origami phononic structures, J. Sound Vib. 430 (2018) 93–100. https://doi.org/10.1016/j.jsv.2018.05.031.
[83] T. Cambonie, E. Gourdon, Innovative origami-based solutions for enhanced quarter-wavelength resonators, J. Sound Vib. 434 (2018) 379–403. https://doi.org/10.1016/j.jsv.2018.07.029.
[84] Z. Yifan, F. Fan, F. Shiwang, C. Liyun, D. Krupali, A. Badreddine, Reconfigurable Origami-Inspired Metamaterials for Controllable Sound Manipulation, Phys. Rev. Appl. 12 (2019) 034029. https://doi.org/10.1103/PhysRevApplied.12.034029.
[85] H. Fang, X. Yu, L. Cheng, Recon fi gurable origami silencers for tunable and programmable sound attenuation, Smart Mater. Struct. 27 (2018) 95007. https://doi.org/10.1088/1361-665X/aad0b6.
[86] A. Benouhiba, P. Rougeot, N. Andreff, K. Rabenorosoa, M. Ouisse, Origami-based auxetic tunable Helmholtz resonator for noise control, Smart Mater. Struct. 30 (2021) 035029. https://doi.org/10.1088/1361-665X/abe180.
[87] R. Diamant, I. Shahar, T. Rosenberg, A. Weiss, Origami-Inspired Adaptive Acoustic Tank for Optimal Reflection Mitigation, IEEE Sens. J. 20 (2020) 15193–15203. https://doi.org/10.1109/JSEN.2020.3011225.
[88] K. Sakagami, T. Okuzono, H. Suzuki, N. Koyanagi, M. Toyoda, Application of Paper Folding Technique to Three-Dimensional Space Sound Absorber with Permeable Membrane : Case Studies of Trial Productions, Int J Acoust Vib. 25 (2020) 243–247. https://doi.org/10.20855/ijav.2020.25.21657.
[89] X. Yu, H. Fang, F. Cui, L. Cheng, Z. Lu, Origami-inspired foldable sound barrier designs, J. Sound Vib. 442 (2019) 514–526. https://doi.org/10.1016/j.jsv.2018.11.025.
[90] S. Babaee, J. Overvelde, E. Chen, V. Tournat, S. Babaee, J. Overvelde, E. Chen, V. Tournat, K.B. Reconfigurable, S. Babaee, J.T.B. Overvelde, E.R. Chen, V. Tournat, K. Bertoldi, Reconfigurable origami-inspired acoustic waveguides, Sci. Adv. 2 (2018). https://doi.org/10.1126/sciadv.1601019.
[91] J.S. Rogers, C. Rohde, A.K. Ikei, M.D. Guild, D.C. Calvo, G.J. Orris, Reconfigurable metasurfaces for directional acoustic sensing, in: Heal. Monit. Struct. Biol. Syst. XII, 2018: p. 106001I. https://doi.org/10.1117/12.2296029.
[92] S. Vyzoviti, N. Remy, Acoustically Efficient Origami Based Partitions for Open Plan Spaces, in: ECAADe 2014, 2014: pp. 487–494. https://doi.org/10.52842/conf.ecaade.2014.1.487.
[93] Y. Yang, Z. You, Geometry of transformable metamaterials inspired by modular origami, J. Mech. Robot. 10 (2018) 1–10. https://doi.org/10.1115/1.4038969.
[94] J.T.B. Overvelde, T.A. De Jong, Y. Shevchenko, S.A. Becerra, G.M. Whitesides, J.C. Weaver, C. Hoberman, K. Bertoldi, A three-dimensional actuated origami-inspired transformable metamaterial with multiple degrees of freedom, Nat. Commun. 7 (2016) 1–8. https://doi.org/10.1038/ncomms10929.
[95] J.T.B. Overvelde, J.C. Weaver, C. Hoberman, K. Bertoldi, Rational design of reconfigurable prismatic architected materials, Nature. 541 (2017) 347–352. https://doi.org/10.1038/nature20824.
[96] J.W. Lee, Y.Y. Kim, Topology optimization of muffler internal partitions for improving acoustical attenuation performance, Int. J. Numer. Methods Eng. 80 (2009) 455–477. https://doi.org/10.1002/nme.2645.
[97] K.F. De Lima, A. Lenzi, R. Barbieri, Topology optimization of muffler internal partitions for improving acoustical attenuation performance, Appl. Acoust. 72 (2011) 142–150. https://doi.org/10.1016/j.apacoust.2010.11.008.
[98] M.C. Chiu, Y.C. Chang, Numerical studies on venting system with multi-chamber perforated mufflers by GA optimization, Appl. Acoust. 69 (2008) 1017–1037. https://doi.org/10.1016/j.apacoust.2007.07.002.
[99] M. Červenka, M. Bednařík, J.-P. Groby, Optimized reactive silencers composed of closely-spaced elongated side-branch resonators, J. Acoust. Soc. Am. 145 (2019) 2210–2220. https://doi.org/10.1121/1.5097167.
[100] M. Sandberg, M. Sjöberg, The use of moments for assessing air quality in ventilated rooms, Build. Environ. 18 (1983) 181–197. https://doi.org/https://doi.org/10.1016/0360-1323(83)90026-4.
[101] C.C. Federspiel, Air-change effectiveness: Theory and calculation methods, Indoor Air. 9 (1999) 47–56. https://doi.org/10.1111/j.1600-0668.1999.t01-3-00008.x.
[102] S. V Patankar, D.B. Spalding, E. Road, a Calculation Procedure for Heat, Mass and Momentum Transfer in Three-Dimensional Parabolic Flows, Int. J. Heat Mass Transf. 15 (1972) 1787–1806. https://doi.org/10.1016/0017-9310(72)90054-3.
[103] X. Wang, X. Luo, B. Yang, Z. Huang, Ultrathin and durable open metamaterials for simultaneous ventilation and sound reduction, Appl. Phys. Lett. 115 (2019). https://doi.org/10.1063/1.5121366.